University of Cyprus
Department of Biological Sciences

Mechanical Cell Membrane stimulation using Magnetic Tweezers increases cell membrane stiffness through integrin dependent and independent mechanisms

ANTONIS MICHANIKOU

A Research-Based Master's Thesis
for the
Degree of Magister Scientiae in Biomedical Sciences

December 19, 2022

ANTONIS MICHANIKOU

ABSTRACT

Several cellular processes, such as proliferation, migration tissue morphogenesis and tissue regeneration, are closely regulated by the cells ability to sense their microenvironment and translate mechanical stimuli to actionable intracellular biochemical signals. Integrins play a crucial role in these mechanotransduction mediated pathways, as they play a critical role linking a cells actin cytoskeleton to the extracellular matrix (ECM) and thus operating as an intracellular and extracellular hotspot of biochemical signals and mechanosensing. The cell's ability to sense ECM characteristics such as stiffness is primarily mediated through Integrins, that relay this information through Focal adhesions and the connection to the actin cytoskeleton. ECM ligands like fibronectin (FN) showcase high affinity binding to integrins receptors through their RGD binding sequence and enable the adhesion of cells to the extracellular matrix. The aim of this study was to address the ability of the cell to sense external mechanical stimuli through integrin dependent and independent mechanotransduction, upon force application to the cell membrane. To address this and be able to exert sufficient forces to deform the cell membrane we constructed a custom-made magnetic tweezer that was able to generate up to 50 nN of force from 5 μm distance on 4.5 μm superparamagnetic beads. We confirmed the magnitude of the applied magnetic field of the magnetic tweezer using previous reported methods and Force-Distance calibration curves. Additionally using a high initial magnetic permeability and low hysteresis soft-alloy core we were able to apply rapid magnetization and demagnetization regimes to the area of interest, thus creating a regime of high magnetic force-pulses with high temporal resolution. Furthermore, we showcased the ability of the magnetic tweezer to apply sufficient forces to displace 4.5 μm superparamagnetic beads embedded in elastic polyacrylamide gels using magnetic pulses followed by relaxation displacements upon rapid demagnetization of the electromagnet. We then applied the same methodology on HeLa cells via Fibronectin and Concanavalin A(CONA) conjugated superparamagnetic beads. We functionalized the superparamagnetic beads using p-toluene-sulfonyl (Tosyl) chemistry resulting in the covalent binding of CONA and FN through primary amine groups on the bead surface. We went on to use live cell imaging to study the displacements of these microspheres upon applied magnetic field

ANTONIS MICHANIKOU

with and without treatment with the actin polymerization inhibitor, Cytochalasin D(CYTO), and the cell contractility inhibitor Rho Kinase, Y-27632 (ROCK). Decreasing displacements of FN coated superparamagnetic beads of a magnitude of -61%($p<0.05$) over time where observed, an effect that was not observed upon treatment of HeLa cells with the CYTO and ROCK. CONA conjugated beads also displayed decreases of a magnitude of -29% ($p<0.05$), but treatment with CYTO and ROCK didn't have an effect, as same magnitude reductions where observed. The above results suggest that PM mechanical stimulation results in the stiffening of the cell through integrin dependent and independent mechanisms. It also suggests that integrin-based stiffening is entirely dependent on the actin cytoskeleton and actomyosin contractility while integrin independent changes in cortical stiffness may reflect changes in PM lipid composition or changes in the polymerization of other cytoskeletal elements such as intermediate filaments.

ANTONIS MICHANIKOU

DEDICATION

To my family

ACKNOWLEDGEMENTS

I would like to thank my thesis supervisor Dr. Paris Skourides, for being patient with me and always willing to help, also all the members of The Skourides Lab past and present, and especially Dr Aigli Evryviadou and Dr. Rania Hadjisavva.

ANTONIS MICHANIKOU

COMPOSITION OF THE EXAMINATION COMMITTEE

Thesis Supervisor (Examination Committee coordinator): Dr. Paris Skourides, Professor, University of Cyprus

Committee Member: Dr. Vasileios Promponas, Associate Professor, University of Cyprus

Committee Member: Dr. Pantelis Georgiades, Associate Professor, University of Cyprus

ANTONIS MICHAILIKOU

SEMINAR ANNOUNCEMENT

University of Cyprus
Department of Biological Sciences

Master Research Dissertation in Biomedical Sciences (BIO 830/600)

Student Presentation

Monday, 19 December 2022 at 12:00
Building ΧΩΔ01, Room 005, Panepistimioupoli Campus

This seminar is open to the public

Michanikou Antonis

Thesis Supervisor: Prof. Paris Skourides

"Mechanical Cell Membrane stimulation using Magnetic Tweezers increases cell membrane stiffness through integrin dependent and independent mechanisms"

Several cellular processes, such as proliferation, migration tissue morphogenesis and tissue regeneration, are closely regulated by the cells ability to sense their microenvironment and translate mechanical stimuli to actionable intracellular biochemical signals. Integrins play a crucial role in these mechanotransduction mediated pathways, as they play a critical role linking a cells actin cytoskeleton to the extracellular matrix (ECM) and thus operating as an intracellular and extracellular hotspot of biochemical signals and mechanosensing. The cell's ability to sense ECM characteristics such as stiffness is primarily mediated through Integrins, that relay this information through Focal adhesions and the connection to the actin cytoskeleton. ECM ligands like fibronectin (FN) showcase high affinity binding to integrins receptors through their RGD binding sequence and enable the adhesion of cells to the extracellular matrix. The aim of this study was to address the ability of the cell to sense external mechanical stimuli through integrin dependent and independent mechanotransduction, upon force application to the cell membrane. To address this and be able to exert sufficient forces to deform the cell membrane we constructed a custom-made magnetic tweezer that was able to generate up to 50 nN of force from 5 μm distance on 4.5 μm superparamagnetic beads. We confirmed the magnitude of the applied magnetic field of the magnetic tweezer using previous reported methods and Force-Distance calibration curves. Additionally using a high initial magnetic permeability and low hysteresis soft-alloy core we were able to apply rapid magnetization and demagnetization regimes to the area of interest, thus creating a regime of high magnetic force-pulses with high temporal resolution. Furthermore, we showcased the ability of the magnetic tweezer to apply sufficient forces to displace 4.5 μm superparamagnetic beads embedded in elastic polyacrylamide gels using magnetic pulses followed by relaxation displacements upon rapid demagnetization of the electromagnet. We then applied the same methodology on HeLa cells via Fibronectin and Concanavalin A(CONA) conjugated superparamagnetic beads. We functionalized the superparamagnetic beads using p-toluene-sulfonyl (Tosyl) chemistry resulting in the covalent binding of CONA and FN through primary amine groups on the bead surface. We went on to use live cell imaging to study the displacements of these microspheres upon applied magnetic field with and without treatment with the actin polymerization inhibitor, Cytochalasin D(CYTO), and the cell contractility inhibitor Rho Kinase, Y-27632 (ROCK). Decreasing displacements of FN coated superparamagnetic beads of a magnitude of -61%($p<0.05$) over time where observed, an effect that was not observed upon treatment of HeLa cells with the CYTO and ROCK. CONA conjugated beads also displayed decreases of a magnitude of -29% ($p<0.05$), but treatment with CYTO and ROCK didn't have an effect, as same magnitude reductions where observed. The above results suggest that PM mechanical stimulation results in the stiffening of the cell through integrin dependent and independent mechanisms. It also suggests that integrin-based stiffening is entirely dependent on the actin cytoskeleton and actomyosin contractility while integrin independent changes in cortical stiffness may reflect changes in PM lipid composition or changes in the polymerization of other cytoskeletal elements such as intermediate filaments.

TABLE OF CONTENTS

ANTONIS MICHANIKOU

INTRODUCTION

Mechanosensing-Mechanotrasduction

The microenvironment of a cell plays a crucial role in mediating several intracellular processes that are affecting proliferation, differentiation, and tissue growth (Chen, Ju et al. 2017).Mechanosensing refers to the ability of cells to sense mechanical stimuli from their environment and mechanotrasduction refers to their potential to transmit those signals intracellularly to actionable processes (De Belly, Paluch et al. 2022), these events can be mediated through a receptor, mechanosensitive ion channels, or between cell to cell interactions, (Yap, Duszyc et al. 2018) (Chen, Ju et al. 2017). Physical properties of the extracellular matrix (ECM), like stiffness can increase tumor growth, by increasing the actin cytoskeleton tension, through integrin dependent Rho activation, thus promoting Focal Adhesion formation and GF mediated ERK activation (Paszek, Zahir et al. 2005). Mechanical force alterations can also be transduced intracellularly through F-actin by E-cadherin, a-catenin, and b catenin complexes at cell-to-cell adhesion sites, regulating the organization, morphogenesis, and integrity of the epithelium (Paszek, Zahir et al. 2005, Pannekoek, de Rooij et al. 2019). Mechano sensation and transduction is versatile and multiplex process as signaling from the outside in or inside outside may concur simultaneously, for example at focal adhesions the clusters of integrins receive signals in a bidirectional way, this provides to the cell the ability to constantly regulate and adapt to their microenvironment (Roca-Cusachs, Conte et al. 2017). Mechanosensitive gated ion channels have emerged the last years as an extremely fast responsive mechanism to applied external force, through rapid conformational change from closed to open (Roca-Cusachs, Conte et al. 2017, Ridone, Vassalli et al. 2019). A member of these channels, the TREK-2 has been recently reported that upon membrane stretching, these channels take their open conformation, letting ions and solubles intracellularly, transducing the extracellular mechanical stimuli (Clausen, Jarerattanachat et al. 2017).

ANTONIS MICHANIKOU

Actin

Actin in most eukaryotic cells has a concentration above 100Mm, with the ability to undergo polymerization and form helical filaments, it creates a dynamical and multiplex cytoskeletal network (Higgs 2001) with different constructs, of parallel and antiparallel actin filaments, contractile and viscoelastic components (Blanchoin, Boujemaa-Paterski et al. 2014). Actin can be found in two distinct states, the Filamentous actin (F-actin) and the monomeric globular form (G-actin) (Dominguez, Holmes 2011). G-actin is 42-kDa protein, the concertation and the availability in free form monomers is highly corelated with the rapid elongation of F-actin (Visa, Percipalle 2010) . Actin polymerization takes place at the plus end of the actin filament while depolymerization takes place at the minus end (**Figure 1)**, a procedure that is called filament treadmilling (Bugyi, Carlier 2010)**.**

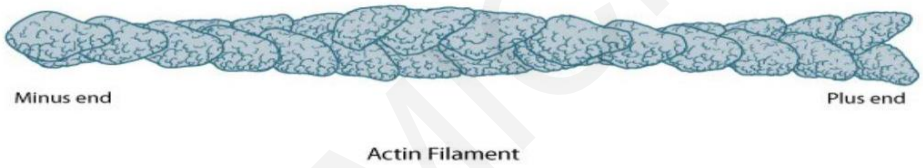

Figure 1: (Adapted from: What are actin filaments? | MBInfo (mechanobio.info) [Accessed on 23/11/2022]

Adenosine 5′-triphosphate (ATP) is a main part of actin structure and function. Upon polymerization and thus elongation of the F-actin, the initial parts (actin monomers) of the structure at the minus end, are hydrolyzed to ADP and Pi creating ADP-actin while the new incorporated actin monomers are bound with ATP **(Figure 2)** (Kudryashov, Reisler 2013). The transition between the G-actin and F-actin, regulated by ATP hydrolysis, creates the foundation for the cytoskeletal network reorganization (Durer, Kudryashov et al. 2012).

ANTONIS MICHANIKOU

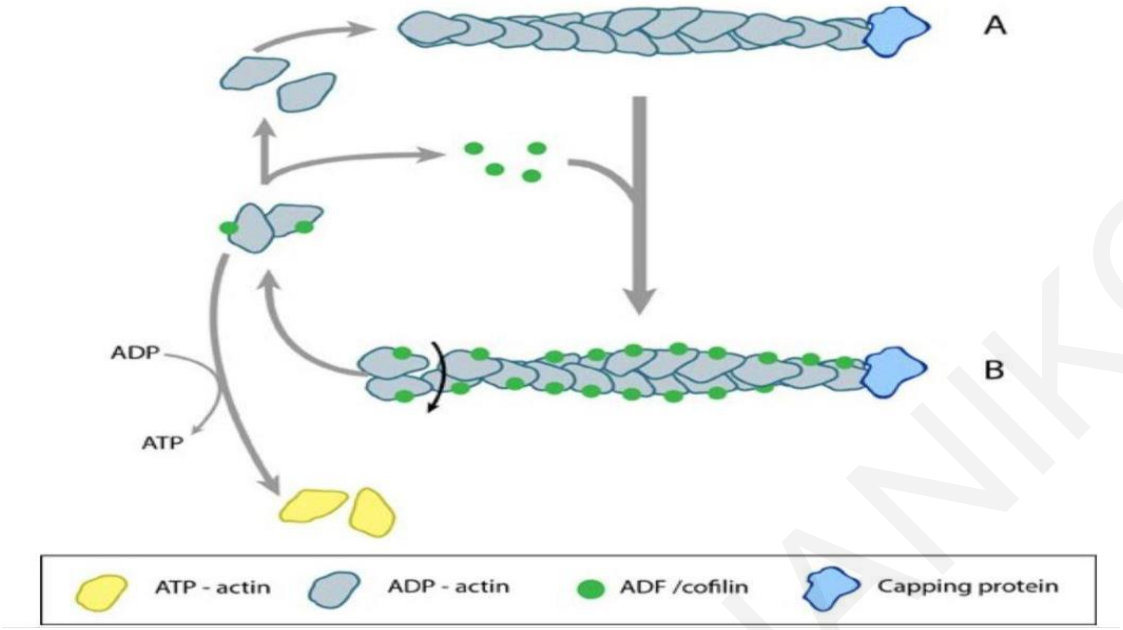

Figure 2: (Adapted from: How do actin filaments depolymerize?| MBInfo (mechanobio.info) [Accessed on 23/11/2022])

While actin polymerization is not thermodynamically favorable the formation of trimers of actin monomer can cause the rapid formation of F-actin (Durer, Kudryashov et al. 2012, Blanchoin, Boujemaa-Paterski et al. 2014). Proteins that show high affinity with actin are remarkably diverse, the interactions between specific proteins such as ADF/cofilins, profilins, formins and capping proteins (gelsolins, b-actinin, CapZ) with actin play a key role of regulating not only the length of the filament but the spatial assembly of actin**.** (Bugyi, Carlier 2010, Sun, H. Q., Wooten et al. 1994, Caldwell, Heiss et al. 1989). To regulate the treadmilling effect, an equilibrium state between monomer ADP-actin disassembly during depolymerization at the minus end and monomer ATP-actin assembly during polymerization at the plus end of the filament must be established (Pollard, Blanchoin et al. 2000). Capping proteins (CP) like gelsolins have a high affinity binding for the plus end (barbered end) of F-actin, thus preventing the elongation of F-actin in that direction (**Figure 2A**) (Edwards, Zwolak et al. 2014). With the binding of CP proteins on actin filaments the binding affinity of other family of proteins ADF/cofilins is enhanced. Cofilin has a higher affinity for ADP-actin, found in the in minus end (pointed end) of F-actin (Shoji, Ohashi et al. 2012), is an important regulator of actin dynamics and reconstruction, as it serves as a dismantle factor for the actin filaments (Blanchoin, Boujemaa-Paterski et al. 2014). The dissociation of ADP-actin monomers by the effects of CP proteins and cofilin, recycles the availability of

ANTONIS MICHANIKOU

available actin ADP-monomers, and with the substitution of the bound ADP with ATP generates the ATP-actin monomer (**Figure 2C**) (Shekhar, Carlier 2017).

Unprompted polymerization of actin ATP-actin monomers in physiological conditions, in concentrations above 100 μM, can form dimers and trimers and filaments in a matter of seconds (Pollard, Blanchoin et al. 2000). The irrepressible polymerization of actin is controlled by profilin, by inhibiting the formation of the dimers and trimers, by binding and blocking the area that monomers of actin can joined together (Dominguez, Holmes 2011). Interestingly while profilin is inhibiting the uncontrollable formation of actin filaments, it can also function as a regulatory factor of the elongation of an actin filament. Cooperativity effects of profilin with other proteins like formin and other contributing factors like APC-C dimer, play a crucial role in the elongation of the F-actin, as they can increase the polymerization rate of the filament, by using profilin as an adaptor protein, thus mediating the elongation (**Figure 3**) (Zweifel, Courtemanche 2020). Importantly, it must be noted that ADP-actin and ATP-actin monomers can both act as polymerization building blocks in both barbered and pointed end, but the rate of polymerization is lower for ADP-actin (Pollard 1984), additionally the elongation at the barbered end exhibits faster rates than the pointed end of the actin filament (Carlier, Pantaloni 1988). The different rates of dissociation between ADP and ATP actin preserves the phenomenon of treadmilling as the critical concentration between free G-actin monomers and actin filaments must be regulated, thus creating a steady state between the available building blocks of cytoskeleton reorganization (Cooper 2000). The regulation of actin polymerization plays a critical role, as it creates structural components with different characteristics throughout the cell interacting with other proteins and creating elaborate constructs (Blanchoin, Boujemaa-Paterski et al. 2014). These complicated networks though they are constructed throughout the cell cycle over time, and some are only observable at specific phases, for example the contractile ring (actomyosin based structure) it is assembled during the anaphase (Skau, Waterman 2015), and must not be confused with the impulsive assembly, polymerization and depolymerization of actin, that either extends/reducing the actin filaments or creating in some extend, unorganized actin filaments (Blanchoin, Boujemaa-Paterski et al. 2014).

ANTONIS MICHAILIKOU

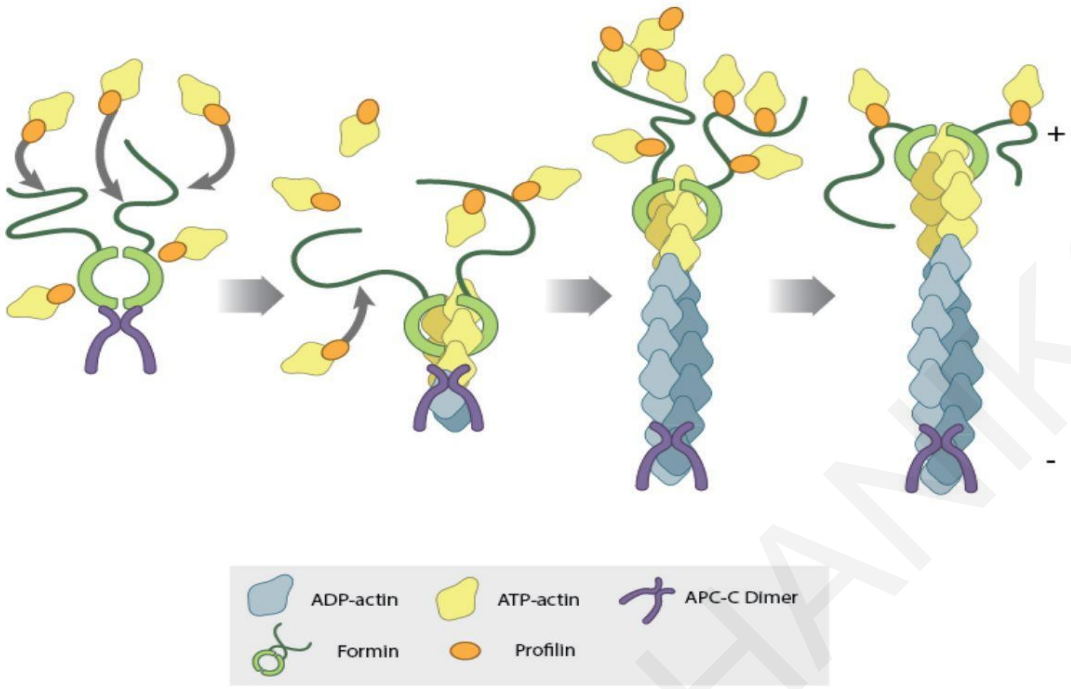

Figure 3: (Adapted from: What is the role of formin in actin polymerization?| MBInfo (mechanobio.info) [Accessed on 23/11/2022])

Myosin

The cytoskeleton is a very complex network and it's not defined only by the complex network of actin filaments and intermediate filaments (Hohmann, Dehghani 2019). Myosin is another protein important to the cytoskeleton, it belongs to the family of motor proteins, due to their structure they can utilize the energy provided by ATP hydrolysis to produce forces and thus facilitate movement (Syamaladevi, Spudich et al. 2012). With forty different genes and twenty definite classes the superfamily of motor proteins interacts with the actin cytoskeleton creating a contractile network that can create tension across the cell (Hirata, Gupta et al. 2015). While different variations of myosin exist, nevertheless they all have key similarities, they consist of a highly conserved head domain (80-kDa) with around 780 amino acids, that includes an actin binding area, this domain is found at the amino terminal of the myosin (Toyoshima, Kron et al. 1987). At the carboxyl terminal of myosin is the tail domain, on the contrary with the N-terminus the variability of this domain is extensive, with many different subtypes thus affecting not only the number of possible isoforms of myosin but also their functionality, as it determines the

ANTONIS MICHAILIKOU

number of head domain of the isoform (Trivedi, Nag et al. 2020, Syamaladevi, Spudich et al. 2012). Important class of myosin in non-muscle cells is the Myosin II (NM II) that undergoes structural conformation under phosphorylation, thus promoting the assembly of actin filaments **Figure 4b** (Aguilar-Cuenca, Llorente-González et al. 2020). It consists of two homologous heavy chains that start from the C-terminus with a long a-helix tail conformation and ends at the N-Terminus with 2 globular head domains, that form a dimer, the dimerization of the two heavy chains leads coil around each other and induce a coil-coil interaction (Rahmani, Ma et al. 2021),the structure is stabilized with 4 lights chains, 2 essential light chains (ELCs) and 2 regulatory light chains (RLCs), that are bound to the C-terminus of the myosin **Figure 4a** (Vicente-Manzanares, Ma et al. 2009).The two a-helix Myosin tails couple up to from bipolar thick myosin filaments, constructing a bundle of myosin dimers (Ojima 2019). The two globular head domains of NMII, both have two distinct binding sites one for ATP and the other for actin in the compact conformation both binding sites are inhibited. When there is no phosphorylation to the regulatory light chains the NMII takes a more compact conformation thus inhibiting its ability to bind to other myosins and actin (Shutova, Yang et al. 2012).

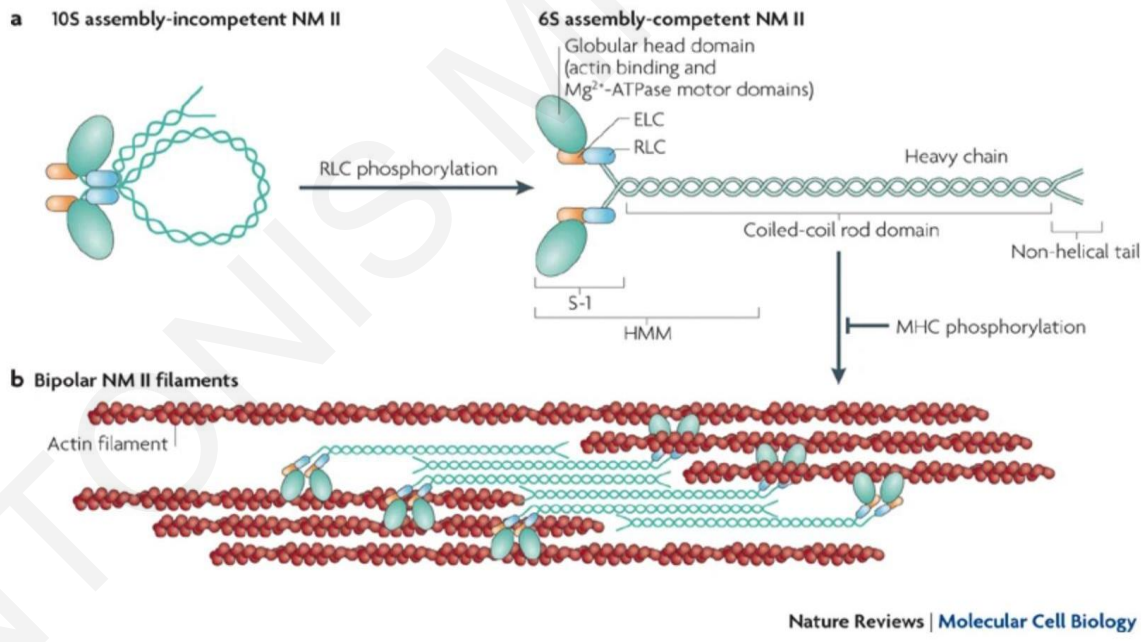

Figure 4: a) Myosin II can take two distinct conformations, the 10S assembly, that is characterized by the interaction of the two globular head domains and the tail, creating a more compact structure, with a high inhibition of the ATPase activity and actin binding.

ANTONIS MICHANIKOU

b) Myosin dimers are forming bundles of NMII with their long tails and the globular heads are bound through their actin binding domain to actin filaments.

Courtesy of: (Vicente-Manzanares, Ma et al. 2009).

The combine effects of the organization of Myosin (NMII) and actin filaments can be found in several cellular components and structures like sarcomeres, ventral stress fibers and the actin cortex (Lehtimäki, Rajakylä et al. 2021). Myosin bundles that are connected to F actin create the power stroke effect (Fischer, Windshugel et al. 2005). The catalytic side of the NMII upon ATP hydrolysis is sliding towards the plus end of F-actin, when the NMII bundles are connected to bidirectional actin filaments the sliding creates the contraction, a highly conserved mechanism that can be found in most cell types (Shutova, Yang et al. 2012).

Intermediate filaments

While the actin filaments have an approximately diameter of about 7 nm, intermediate filaments (IF)exhibit an increase of their diameter to approximately 10 nm, their most important characteristic that differentiate them from other cytoskeletal structures like microtubules and actin filaments is that the proteins that construct the IF are encoded by no less than 73 genes in humans (Dutour-Provenzano, Etienne-Manneville 2021). Similarities in the structure of IF are conserved across all proteins of intermediate filaments as they consist of α-helical rod connected with a non-a helical N-head and Carboxyl terminal- tail domains (Herrmann, Strelkov et al. 2009). In human epithelial cells the intermediate filaments consist mainly of equal amounts of Type I and type II keratins, and form coiled to coil dimers through the central α-helical rod, but the final structure of the intermediate filaments is not conserved because of the variability between the proteins and other IF proteins, type of tissue, and general state of the cell (Jacob, Coulombe et al. 2018). The spatial and structural composition of the IF plays a critical role in the durability of epithelial cells as many studies had demonstrated that Keratin intermediate filaments are essential and provide protection to the cell during applied stress (Geisler, Leube 2016), while other studies shown that intermediate filaments networks of vimentin can retain their maximum elasticity after applied stress (Goldman, Grin et al. 2008). Expression of vimentin

ANTONIS MICHAILIKOU

is mainly observed in specialized glial cells like astrocytes, endothelial cells, and fibroblasts (Hohmann, Dehghani 2019).

Integrins

The adhesion of cells to the extracellular matrix is mediated via transmembrane proteins called integrins (BUCK, Horwitz 1987). The role of this family of proteins is far more complex though, they function as transmembrane non-covalently associated heterodimers with the ability to receive and transduce mechanical and biochemical stimuli throughout the cell via the cell's cytoskeleton and vice versa, constituting an essential role in cell development and tissue organization. For example, adhesion of the cell to the extracellular matrix can produce structures like ventral stress fibres through integrin activation (Santa-Cruz Mateos, Valencia-Expósito et al. 2020). Upon integrin activation one of the pathways that is activated is the RhoA pathway, which mediates the actin polymerization and the integrity of the actin filaments through the RhoA activated formin mDAi (Watanabe, Madaule et al. 1997), the signalling cascade also activates NMII leading to an overall increasing tension (Burridge, Guilluy 2016).

The main structural components of integrins are the alpha (α) and beta (β) glycoprotein subunits, in humans α subunit exhibits a variance of 18 subunits while the β subunit has eight known isoforms, able to construct thus far 24 heterodimers (Takada, Ye et al. 2007). Each heterodimer has a specific ligand affinity, from Arg-Gly-Asp (RGD) peptide specificity to collagen, leukocyte and laminin receptors **Figure 5**. Additionally, the expression of the heterodimers varies throughout the different tissues. Both α and β subunits exhibit conserved domains among their different subunits. The cytoplasmic tails of α and β subunits are rather short and generally consist of twenty to seventy amino acids (Morse, Brahme et al. 2014). The β cytoplasmic tails play a crucial role in integrins intracellular interactions as they have three highly preserve NXXY/F motifs, that bind intracellularly with a vast pool of proteins, thus transducing any extracellular and intracellular signal (Anthis, Campbell 2011).

ANTONIS MICHANIKOU

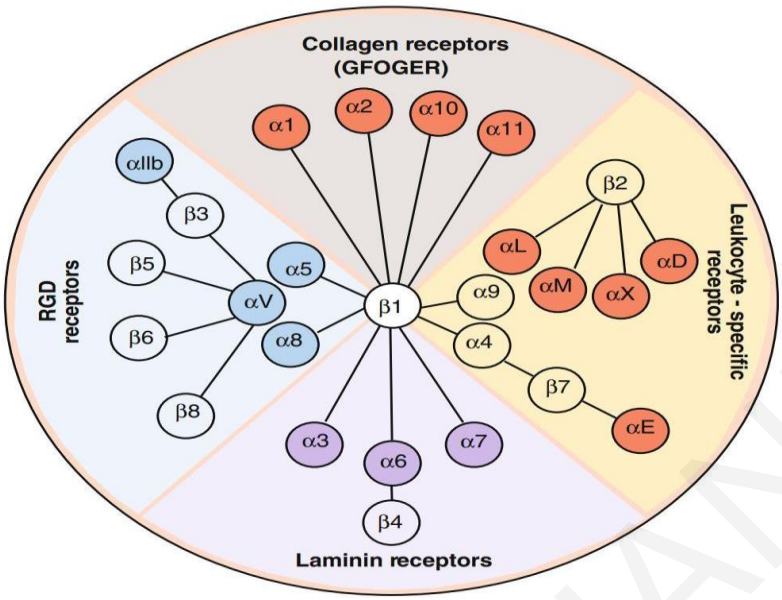

Figure 5: Representation of the various affiliations between subunits α and β and their ligand binding specificity. Courtesy of: (Barczyk, Carracedo et al. 2010)

The closest to the membrane motif mediates the binding for a group of protein family called talins, and the other motif that is further from the membrane acts as a binding site for kindlins, the third motif is in the centre of the two motifs, and it consist of a threonine and serine (T/S) sequence **Figure 6** (Gahmberg, Grönholm et al. 2022). The α cytoplasmic tail consists of only one close to the membrane motif that is also conserved and has been shown to be a binding site for several proteins like SHARPIN, the binding of this protein keeps the integrin in its inactive conformation (Morse, Brahme et al. 2014, Erusappan, Alam et al. 2019). Phosphorylation of these motifs can protect them from calpain cleavage and more importantly regulated the binding of proteins, for example the phosphorylation of the central T/S motif by a kinase mediate the binding of 14-3-3 proteins but also the phosphorylation inhibits the binding of filamin, thus working as a bidirectional regulation (Morse, Brahme et al. 2014). The transmembrane domains (TM) on both subunits comprise of a hydrophobic a-helix, that creates the anchoring of the heterodimer to the membrane (Wegener, Campbell 2008). The elongated ectodomains of the heterodimer consist of 700 to 1000 amino acids (Danen 2013)and mediated the binding of ligands from the ECM (Lietha, Izard 2020).

ANTONIS MICHANIKOU

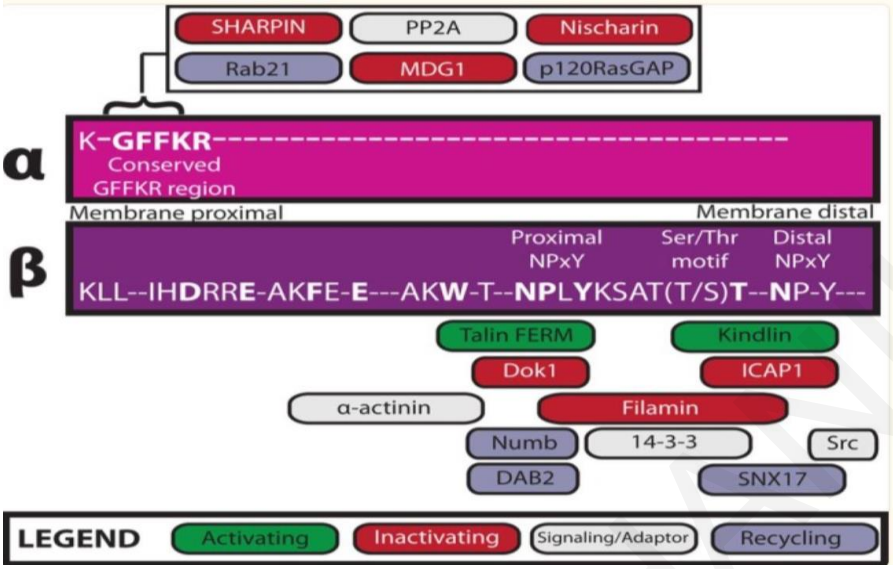

Figure 6: Representation of the two cytoplasmic tails of integrins and their binding sites. Courtesy of: (Morse, Brahme et al. 2014)

The TM domains of the b subunit are connected to 4 cysteine repeated integrin epidermal growth factors (I-EGF-1, I-EGF-2, I-EGF-3, I-EGF-4) ,followed by a plexin-semaphorin-integrin (PSI) domain, with a hybrid domain and the important βI domain (Yousefi, Vatanmakanian et al. 2021).The βI domain is crucial as it is consists of a metal-ion-dependent adhesion site(MIDAS), containing a magnesium cation (Mg^{2+}),this site is specific for ligand binding **Figure 7B** (Craig, Gao et al. 2004),and next to MIDAS the adjacent metal-ion-dependent adhesion site(ADMIDAS) that is activated by Mn^{2+} and inhibited by Ca^{2+} ,thus regulating the binding of the ligand (Mould, Barton et al. 2003).Respectively for the α subunit ,the TM are connected through two calves domains ,Calf1 and Calf2,followed up by the thigh domain (Barczyk, Carracedo et al. 2010). A full schematic of the integrin structure with the domains is shown in **Figure 7**. Accordingly, the crucial domain for ligand binding is the αI, it can be found inside of a seven bladed β-propeller domain that has calcium binding motifs that follows the thigh domain (Oxvig, Springer 1998).

ANTONIS MICHAILIKOU

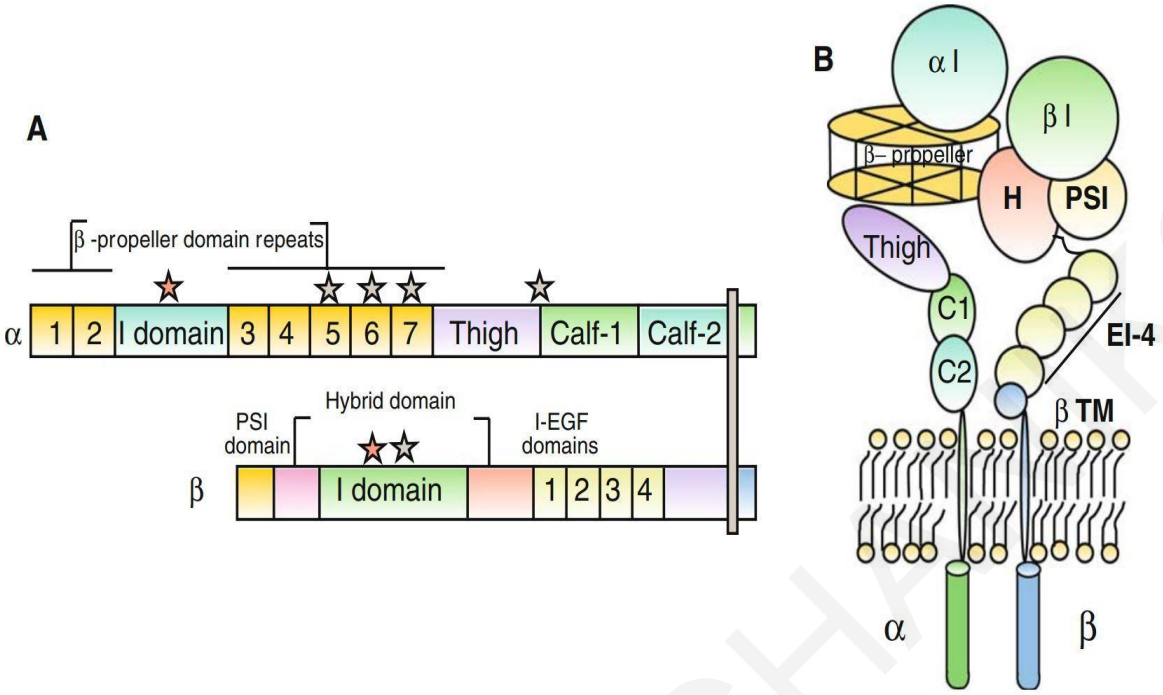

Figure 7: Schematic representation of the arrangement of different domains of integrins.

Courtesy of: (Barczyk, Carracedo et al. 2010)

Similar as in the βI domain, the MIDAS adhesion site is also present, and it facilitates the ligand binding to the ECM (Danen 2013). While important the αI domain is not conserved across different α subunits, with α3 to α9, αV and αIIb subunits are lacking this specific domain (Chouhan, Denesyuk et al. 2011). In heterodimers that are lacking this domain the ligand binding is mediated by the βI domain of the β subunit via the MIDAS adhesion site with the synergistic activity of the β propeller of the α subunit that stabilizes the interactions between the integrin ectodomain and the ligand **Figure 8A** (Chouhan, Denesyuk et al. 2011). An example of this interaction is the ligand specific affinity on integrins heterodimers with the RGD peptide contain proteins like fibronectin. Heterodimers like α5β1, αVβ1, αVβ3, αVβ5, αVβ6, αVβ8, and αIIbβ3 establish their interaction with the ligand via the β subunit and MIDAS site with the carboxylate sidechain of the RGD peptide that can be found in the aspartate residue (Takada, Ye et al. 2007).

ANTONIS MICHAILOU

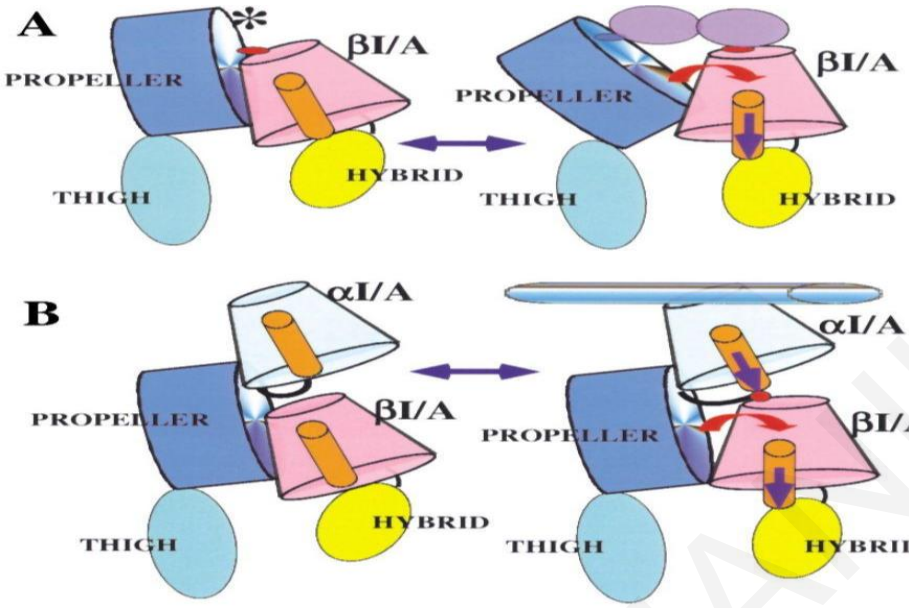

Figure 8: Hypothetical representation of the two different ways for Ligand binding to Integrin Heads heterodimers.

A) Represents the binding of a ligand to the integrins ectodomain head without the αI domain.

B) The binding of ligand through a heterodimer that's has an αI domain.

Courtesy of: (Hynes 2002).

Integrins that are missing the αI domain like, αVβ3 and αIIbβ3 have been studied extensively over the past years, current hallmarks in the integrin conformation through inactive and active state are based on these heterodimers (Xiong, Stehle et al. 2002, Xiong, Stehle et al. 2001, Bachmann, Kukkurainen et al. 2019). The inactive state of the integrin, with low ligand affinity is characterized by two distinct conformational changes, the bending of the headpiece towards the membrane and the transmembrane domains position close to each other (Wegener, Campbell 2008). Upon intracellular activation of the heterodimer, through the binding of proteins to the cytoplasmic tails as previously explain, the integrin undergoes a conformational rearrangement of its domains, resulting to the intermediate affinity state, characterized by an extended close headpiece ectodomain and the separation of the TM domains but in proximity (Shattil, Kim et al. 2010).Similar activation can occur via integrin-ligand interactions from the extracellular matrix (Takagi, Petre et al. 2002, Mehrbod, Trisno et al. 2013). The fully extended high affinity state of

ANTONIS MICHAILIKOU

integrins is define from the fully open headpiece ectodomain with a significant TM domains separation **Figure 9**.

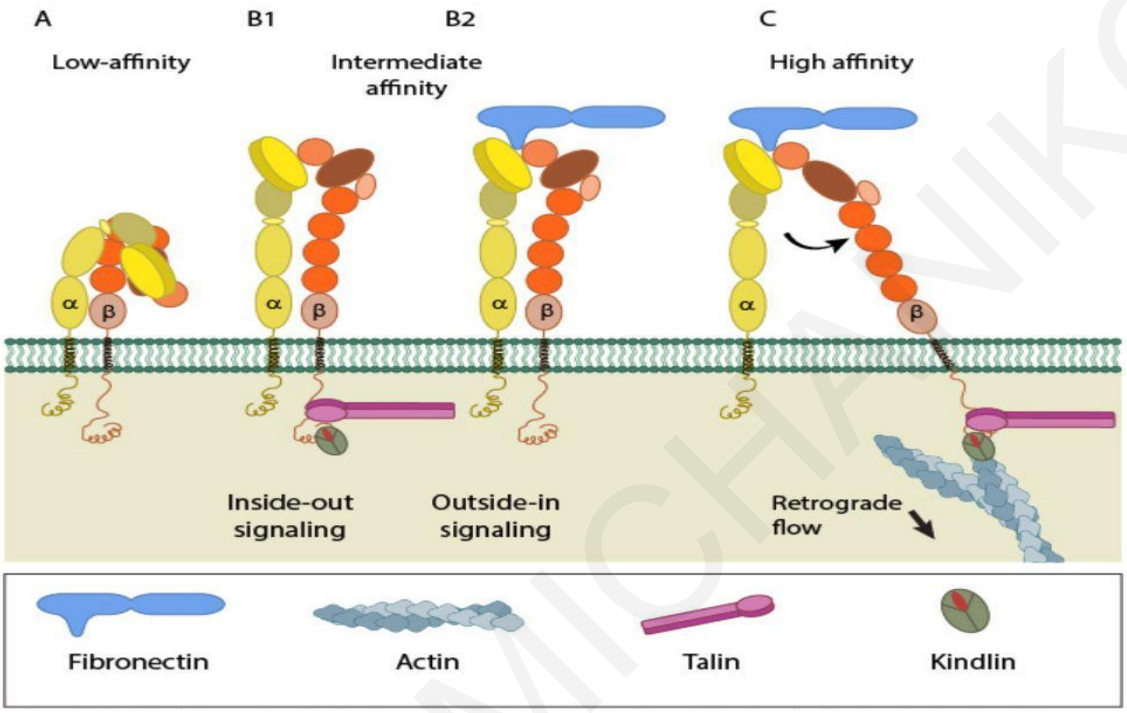

Figure 9: The different states of integrin activation from the bent-low affinity state to the high affinity state(Adapted from: How is integrin activated?| MBInfo (mechanobio.info) [Accessed on 24/11/2022])

Fibronectin

Fibronectin (FN) is composed of Type I, Type II and Type III repeats, all of them containing a pair of antiparallel β-sheets, they are found in the extracellular matrix and can interact with focal adhesion via integrin binding, thus connecting the cytoskeleton with the ECM (Cao, Nicosia et al. 2017). In the blood plasma FN is soluble and its synthesized by hepatocytes, while the ECM fibronectin is less soluble and its synthesizes from fibroblasts (Cao, Nicosia et al. 2017, Parisi, Toffoli et al. 2020).Fibronectin is glycoprotein, that over the last years was study extensively, various binding sites have identified that beyond the RGD peptide that can also facilitate the

ANTONIS MICHANIKOU

binding of FN to integrins some of the sequences are, but are not limited, III10, III9,I_{1-9},$I_{1,2}$ (Pankov, Yamada 2002).

Magnetic Tweezers

The effect of external mechanical stimuli is usually address by several techniques like optical tweezers, aspiration using micropipettes induce stress to elastic substrates via stretch devices and magnetic tweezers (Polacheck, Chen 2016).Magnetic tweezers can take different shapes and sizes their design is subjected to the area of the application, Vertical magnetic tweezers are uses for DNA unfolding experiments, multidimensional magnetic tweezers consist of several poles and are highly versatile, unidirectional magnetic tweezers can exert high forces at the area of interest (Kollmannsberger, Fabry 2007). Unidirectional magnetic tweezers are simple and provide sufficient forces up to 100 nN, they are constructed based on the principle of a simple electromagnet, their design consist of a hollow non-magnetic material that is acting as a frame, through the hollow frame a high magnetic permeability core must be inserted, around the frame a copper wire is wrapped multiple times to create a solenoid, the two ends of the solenoid are then connected to a DC power supply, when current is running through the solenoid it generates the magnetic field (Kollmannsberger, Fabry 2007). This design had been used to address microrheological characteristics of single cells like viscoelasticity and plasticity of the plasma membrane (Bonakdar, Gerum et al. 2016).Other designs have applications to study single molecules like nucleic acids and proteins (Bonakdar, Gerum et al. 2016, Vilfan, Lipfert et al. 2009).

Aims

The main aim of this thesis was to design, build and test a magnetic tweezer that can be used to study cellular responses to external mechanical stimulation. In addition, we wanted to study the responses elicited by deformation of the plasma membrane using mechanical forces, using integrin dependent and independent mechanisms. For these purposes we constructed a working magnetic tweezer that can applied sufficient forces to deform the plasma membrane.

ANTONIS MICHANKOU

MATERIALS AND METHODS

Cells and Cell Culture

HeLa (CCL2, ATCC) in culture at 37°C and 5% CO2, 10% Fetal Bovine Serum (Biosera),1x Antibiotic/Antimycotic solution (Biosera). MDCK (NBL-2, ATCC), in culture at 37°C and 5% CO2, 10% or 2% Fetal Bovine Serum (Biosera),1x Antibiotic/Antimycotic solution (Biosera),

Polyacrylamide gels-Hydrogels

Sonication of glass cover slips for 15 min. Several washes using distilled H_2O, follow by the addition of isopropanol, and air-dried incubation at 65^0 C. Some coverslips were prepared with Rain-X (Water Repellent, 1000 µl each), addition follow up by 2 min incubation. Several washes with distilled H_2O. Polyacrylamide gels of 1kPa and 200 Pa stiffness were prepared **Table 1**. Drop of prepare solution 30 µl + superparamagnetic beads on a clean cover slip followed up by a Rain-X coverslip on top. Incubation for 1 h at room temperature for the gels to set, followed up by incubation with distilled water for 1 h.

Young modulus	**Acrylamide %**	**Bis-acrylamide %**	**Acrylamide from 40% stock solution (ml)**	**Bis-acrylamide from 2% stock solution (ml)**	**Water (ml)**	**Acrylamide from 40% stock solution (µl)**	**Bis-acrylamide from 2% stock solution (µl)**	**Water (µl)**	**1/100 total volume of APS**
200 Pa	1.8	0.018	0.45	0.09	5.46	22.5	4.5	269.7	3
1 kPa	3	0.09	0.75	0.45	4.8	37.5	22.5	236.7	3

Table 1: Polyacrylamide gels recipes in µl for a total of 300 µl mix.

ANTONIS MICHANKOU

Drugs-Inhibitors

Rho-kinase inhibitor, Y-27632, Cytochalasin D (10 μM, 2μM)
Cells were treated with inhibitors 30 min before imaging.

Immunostaining

The cover slips with the cells were washed three times with 1x PBS solution and fixed for 10 minutes using 4% Paraformaldehyde (PFA). They were incubated using 50mM glycine in 1x PBS for 10 minutes in RT. After incubation they were permeabilized using with 0,2% Triton-X 100 in 1x PBS for 10 minutes. Primary antibodies were added in 10% donkey serum in 1x PBS for 1 hour RT/overnight at 4°C. Primary antibodies: β-catenin rabbit (Sino, 11279R021) 1: 1000, ARL13B 1:1000, γ-tubulin Rabbit 1:1000, N-Cadherin mouse (Thermo, MA1-159) 1:300, N-Cadherin rabbit (Sino, 11039-R014) 1:500, a-tubulin Mouse 1:1000,N-Cadherin rabbit (Sino, 11039-R020) 1:500, γ-tubulin Goat 1:1000,ZO-1 Rat 1:100 ,Smo mouse 1:100 (not listed-removed).After the addition washes with 1x PBS (three times for 5-10 minutes), followed up by the secondary antibodies again in 10% donkey serum in 1x PBS) for 1 hour at room temperature. Secondary antibodies that were used: 488 Donkey anti-Mouse (Invitrogen, 1:500), 568 Donkey anti-Rabbit (Invitrogen, 1:500), 647 Donkey anti-Rat (Invitrogen, 1:300), Cy3 Donkey anti-Rat (Jackson, 1:500), 488 Donkey anti-Rabbit (Invitrogen, 1:500). Follow by three washes with 1x PBS. Mounting, with prolong (Invitrogen, P36961) and glass coverslip was flipped on top of it.

Preparation of superparamagnetic beads

Dynabeads M-450 Tosylactivated (Thermo Fisher) were used and prepared for coating according to the manufacturer's protocol for a final concentration of $1.4x10^5$ beads/ml.
Coating with Fibronectin and Concanavalin A was done according to the manufacturers of Dynabeads M-450 protocol stated (200 μg of protein / ml)

ANTONIS MICHANIKOU

Magnetic tweezer

Brass frame with the windings was order based on custom design **Figure 10** from Transfonix LTD (Cyprus Larnana) windings approximately 300 using AWG24 wire

Metal rod: ASTM A 753 TYPE 4, UNS N14080 – MuMETAL

DC Power supply: GRAT-APS3003D (Single 30V,3A, DC Power Supply)

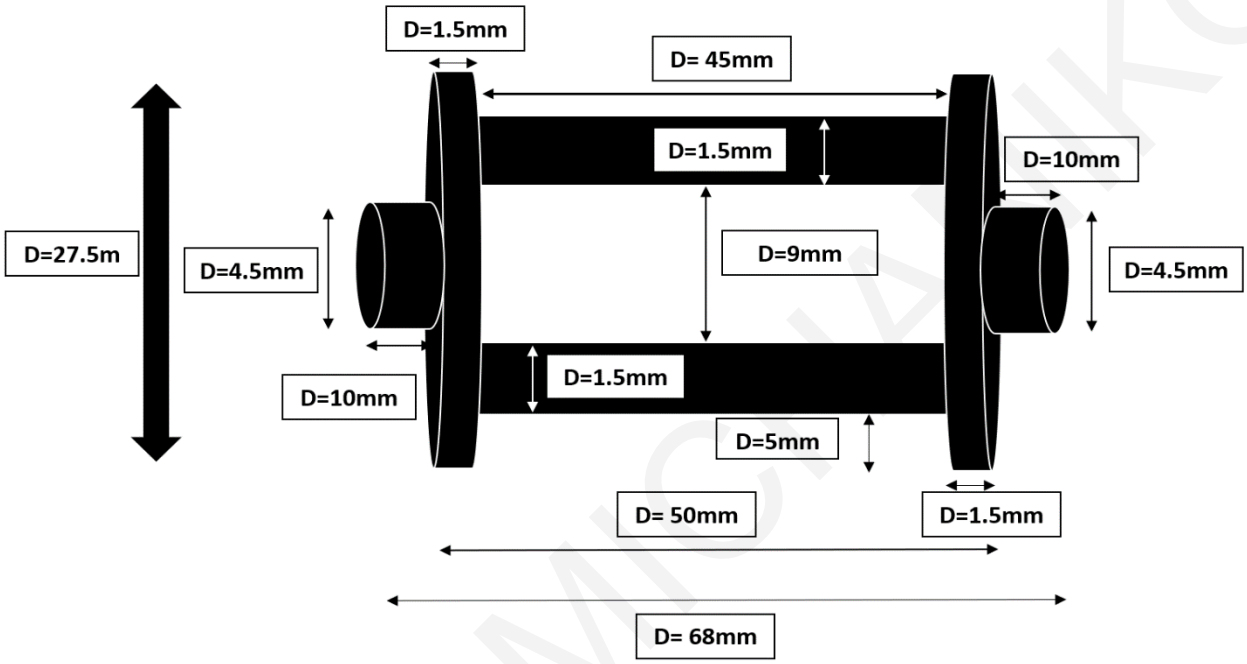

Figure 10: Brass frame with dimensions

In a homogenous magnetic field, the bead should experience a gradient force characterized by:

$$\mathbf{F} = \left(\mathbf{m} \cdot \frac{\partial}{\partial \mathbf{r}}\right)\mathbf{B}.$$

m: magnetic moment

B: Magnitude of applied field

Quantification and Statistical analysis

Manual tracking of the beads was performed using ImageJ.

Calculations, visualizations were done using Excel software.

Statistical analysis was performed with Stata software and Excel Software

Statistical significance was set at p-value < 0.05.

ANTONIS MICHAILIKOU

RESULTS

Magnetic tweezer design

The magnetic tweezer built for the purposes of this thesis was based on the design developed by Philip Kollmabenger (Kollmannsberger, Fabry 2007). It consists of a brass alloy frame ,70 mm in length with a hollow 6 mm inner diameter. Around the brass frame in 3 layers is a 0.511 mm copper wire (AWG24), thus creating a solenoid of approximately ~300 turns. The two ends of the cooper wire from the solenoid are connected to a DC Power supply able to generate up to 3A of electric current. The conductivity of the copper wire, the overall structure of the solenoid and the applied electrical current creates an electromagnet (Tanase, Biais et al. 2007). The extremely low magnetic permeability of the brass frame does not influence in anyway the magnetic field created in the hollow center of the device by the solenoid. For the amplification of the generated electromagnetic field, a soft metal alloy rod was used, 150mm long with a 4.5 mm diameter. The Mu-Metal rode is composed of 80% Nickel, 5% Molybdenum and the balance iron, one end of the metal rod was tapered creating a tip with a radius of 10 μm. The selection of the specific Mu-Metal rod was important as it offers maximum initial high permeability and minimum Hysteresis (Arpaia, Burrows et al. 2021). The electromagnet is adjusted to a micromanipulator for precision control movements from the target site. An image of the magnetic tweezer set up its shown in **Figure 11**. The adjustment of the tweezer to the micromanipulator enables the precise positioning of the rod tip to the area of interest, these instruments already are designed to facilitate precision movements like injections, in the place of the needle we attached the not-tapered end of the metal core. As it was instructed from the manual of the micromanipulator the maximum load on the head must not exceed 100 gr, and it was taken into consideration during the design of the magnetic tweezer. The weight of the rod-brass frame design is approximately 85 gr. In **Figure 12** is a close of the magnetic tweezer that is attached to the micromanipulator.

ANTONIS MICHAILIKOU

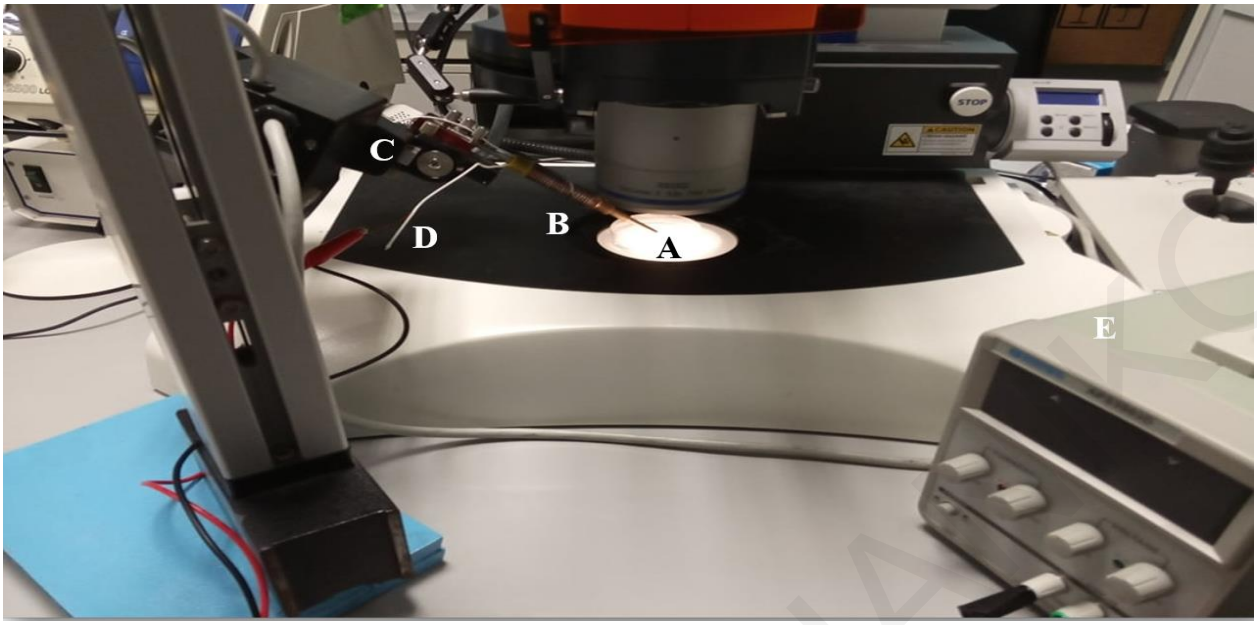

Figure 11: A) Tapered tip of the core material Mu-Metal, B) Brass frame with 300 turns of copper wire, C) Micromanipulator, D) Copper wires without insulation at the end, connected to the E) DC Power supply.

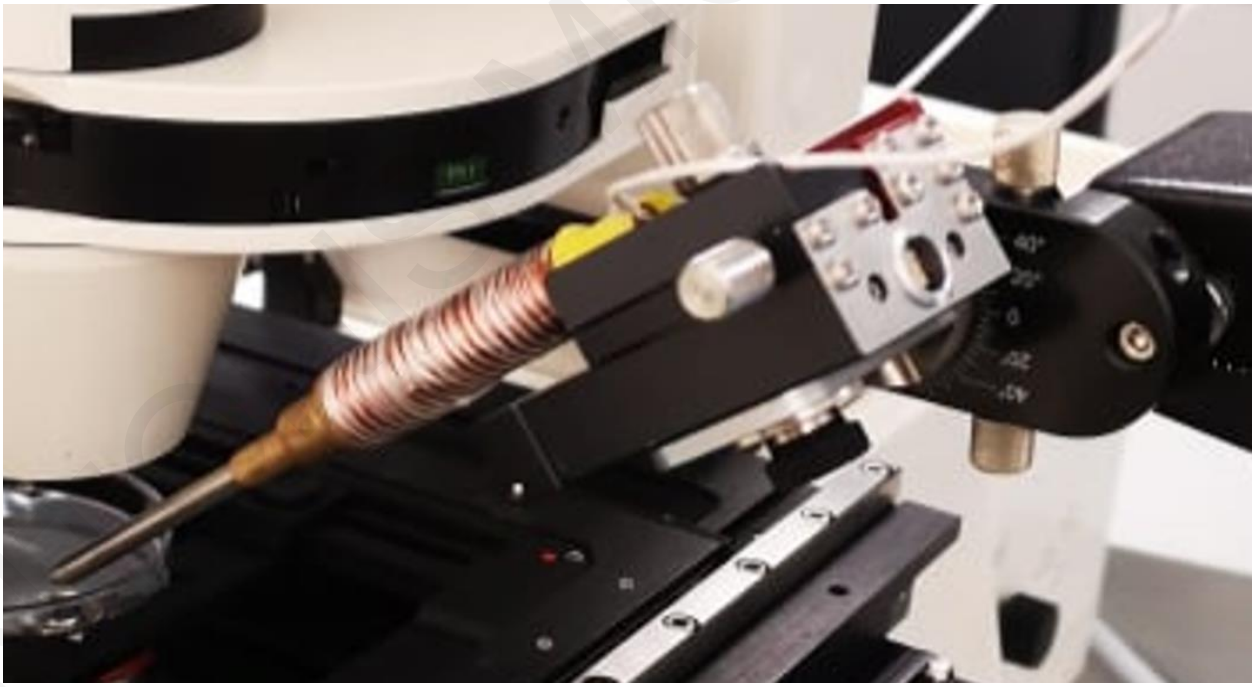

Figure 12: Close up of the magnetic tweezer that shows the brass frame with the windings creating a solenoid. One end of the metal core is attached to micromanipulator and the tapered tip is inserted into glass coverslip in a 45-degree angle.

Calibration of the Magnetic tweezer

Calibration of the magnetic tweezer can be carried out by tracking the movement of magnetic microspheres in high viscosity fluid upon applied magnetic field (Kollmabenger2007). The tapered end of the Mu-Metal rod was submerged in glycerol and 4.5 μm Tosyl activated Dynabeads were added to the viscous fluid. Continuous applied current was introduced to the solenoid using the DC Power supply. The movement of the beads towards the tip of the electromagnet was tracked, the velocity of the beads as well as the distance from the tip in each different frame was calculated with FIJI software. Using the Stokes Formula for viscous drag the force exerted on the beads was calculated,

$$\mathbf{F} = 6\pi \times \eta \times r \times \mathbf{v}$$

F: Applied force

η: Fluid Viscosity

r: radius of the bead

v: velocity of the bead

The equation implies that the force a bead experiences is highly correlated with the distance from the magnetic field, in this case the distance from the tip of the magnetic tweezer.

Plots of the force to distance at three different currents (A) 200 mA, (B) 1000 mA and (C) 3000 mA are displayed in **Figure 13**. Power law curves were accessed via log transformation of the dependent variable (Force) and the independent variable (Distance). Regression analysis was performed using the log transformed data for each of the three different applied currents to access the significance of the variables Table 1. Statistically significant results were found in 200 mA, ($R2 = .90$, $F(1, 117) = 1077$, $p < .000$), 1000 mA, ($R2 = .86$, $F(1, 25) = 152$, $p < .000$) and 3000 mA ,($R2 = .79$, $F(1, 30) = 114$, $p < .000$).

ANTONIS MICHANIKOU

Experiment	Current	b0	p-value(b0)	b1	p-value(b1)
A	200 mA	3.61	p < .000	-0.42	p < .000
B	1000 mA	4.82	p < .000	-0.72	p < .000
C	3000 mA	5.19	p < .000	-0.81	p < .000

Table 1: b0 and b1 coefficients with their calculated p-values for each experiment.

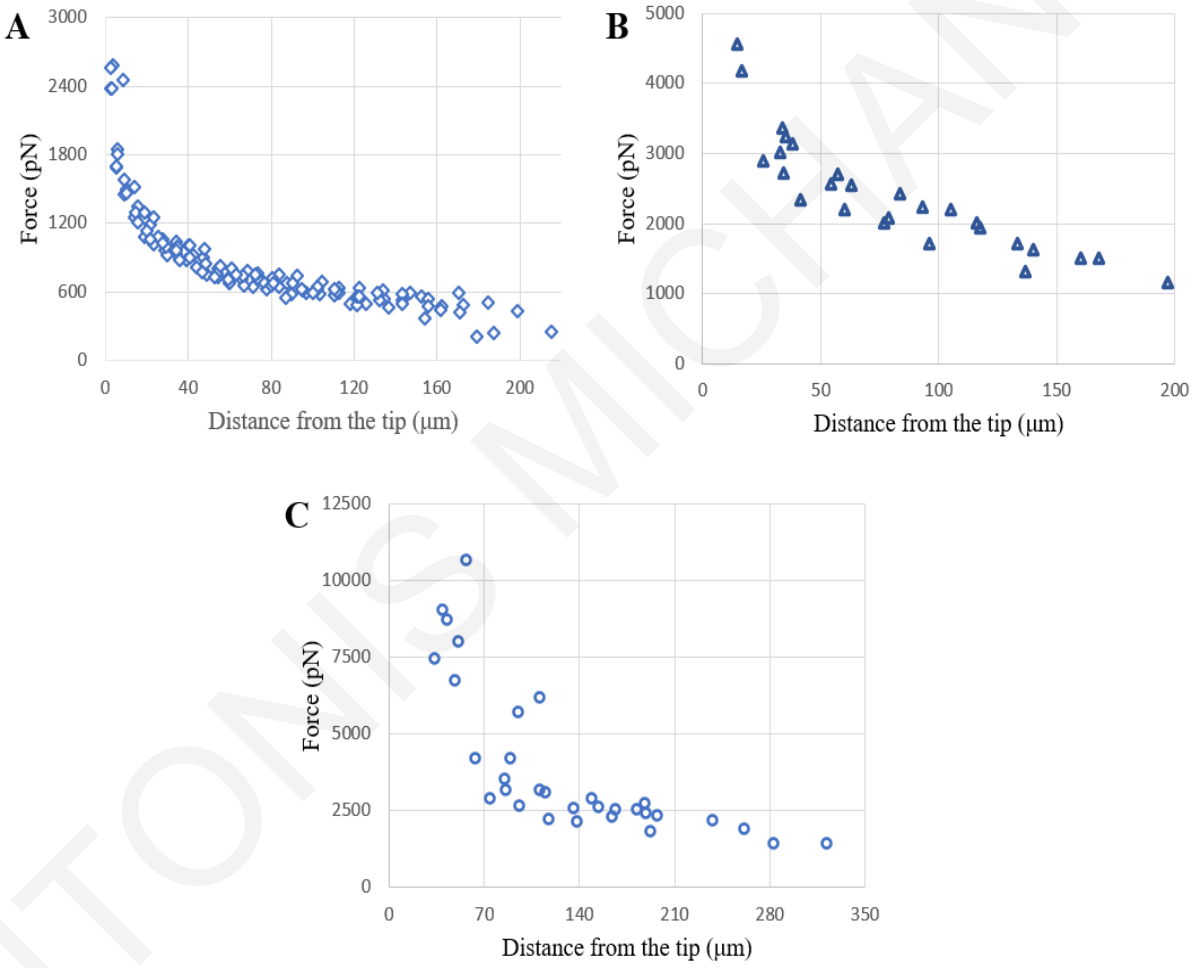

Figure 13: A) Scatter plot of Force- distance calibration when 200 mA of current is applied. B) Scatter plot of Force- distance calibration when 1000 mA of current is applied and C) Scatter plot of Force- distance calibration when 3000 mA of current is applied. Note that the Y axis is in force in pico-Newton and that the bounds of the axis is different in each experiment.

ANTONIS MICHANIKOU

The log transformed coefficients were used to calculate Y variable at fix distances from the tip and then construct the three distinct Force distance calibration curves **Figure 14**. The results imply that the force a bead experience is highly corelated with the distance from the magnetic field in this case the distance from the tip of the magnetic tweezer and the current that runs through the solenoid, upon increasing current and decreasing distance from the tip the beads velocity is increased in a power law manner. These results obtained from this custom designed magnetic tweezer are in full agreement with other studies that also used the same approach to calibrate their tweezers (Kollmannsberger, Fabry 2007, Kah, Dürrbeck et al. 2020)

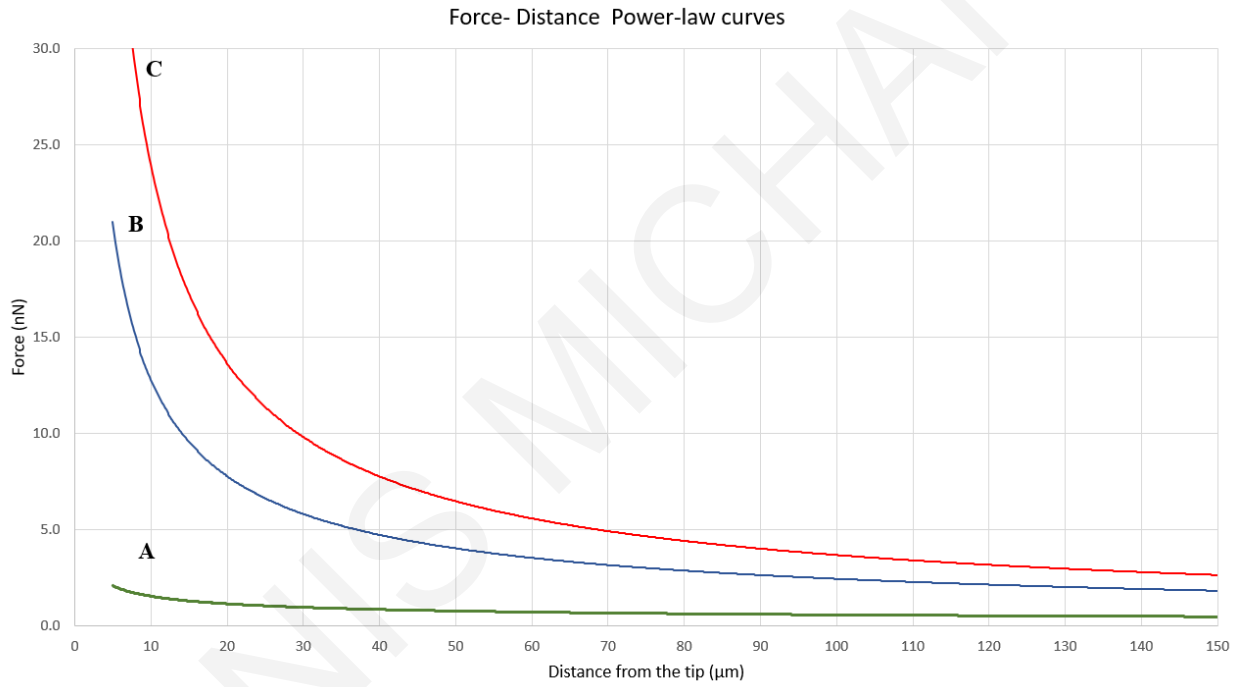

Figure 14: A) Green line represents the calibration curve of force to distance for beads movement when 200 mA is applied to the magnetic tweezer. B) and C) corresponds to applied electrical currents of 1000 and 3000 mA respectively.

Additionally, to test the ability of the Magnetic tweezer to displace superparamagnetic beads on a stiffer substrate, the beads were embedded on the surface of polyacrylamide hydrogels of elastic modulus of 200 Pa and 1000 Pa **Figure 15**, as described in the materials and methods section.

ANTONIS MICHANIKOU

The electric current passing through the solenoid was set to 3000 mA, and a very short pulse ranging from 1-2 seconds was applied creating a magnetic field near the tip of the magnetic tweezer. The tweezer was then turned off, thus removing the applied magnetic field. Bead displacement was measured during and after the pulse **Figure 15**, to distinguish the two displacements the latter is going to be referred to as recoil displacement. For each bead presented in the results distance from the tip was measured (**Figure 16**) before applying the magnetic field and force was calculated based on the calibration Force to Distance curve shown in **Figure 14** for an applied current of 3000 mA. Furthermore, the recoil displacement was used as a quality indicator of the attachment of the bead to the polyacrylamide gel. Beads that weren't displaying any recoil displacement, upon removal of the applied magnetic field, were excluded from the analysis.

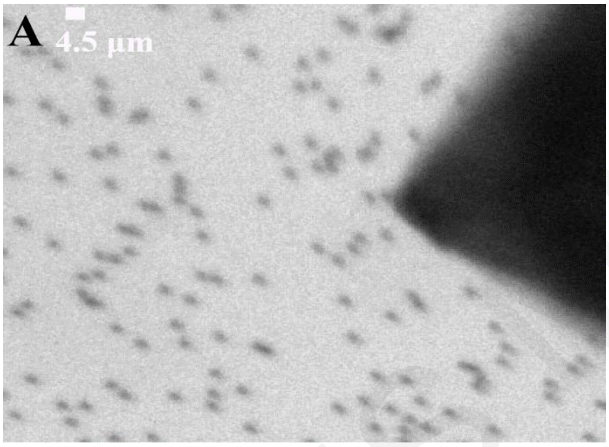

Figure 15: A) 4.5 μm Tosyl activated Dynabeads embedded in 1000 Pa polyacrylamide gel, the magnetic tweezer tip was position in proximity above the gel surface. B) 4.5 μm Tosyl activated Dynabeads embedded in 200 Pa polyacrylamide gel. C) Upper frame displays the bead position before the pulse the second frame the displacement of the bead before the end of the pulse and last frame the position of the bead after stress relaxation of the polyacrylamide gel

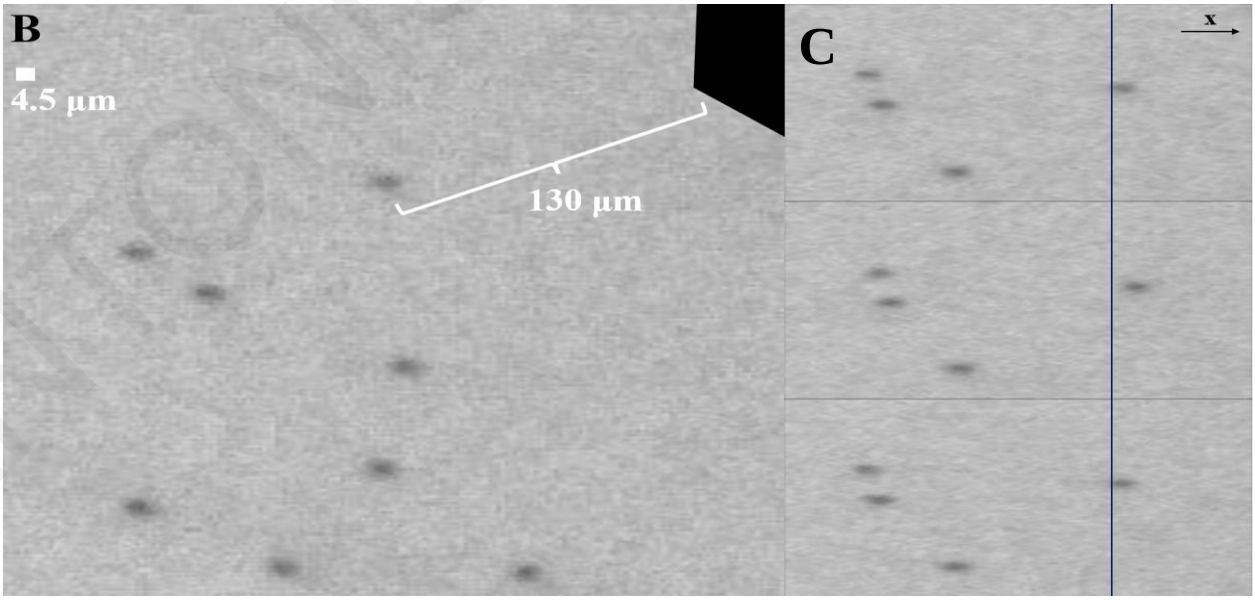

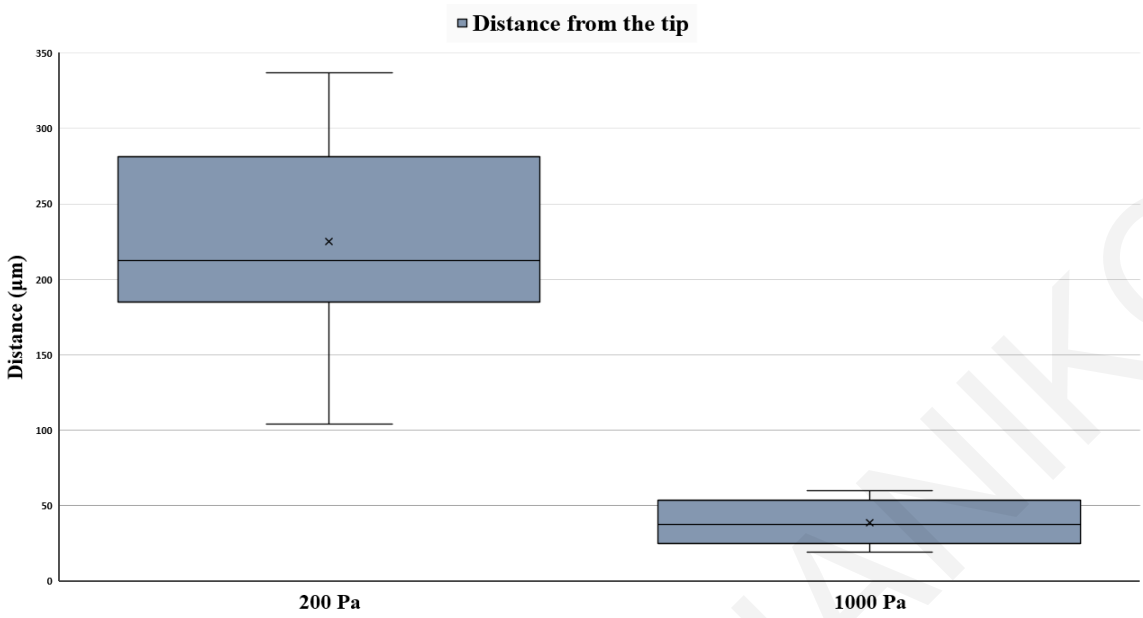

Figure 16: Bead-Magnetic tweezer distance box plot for 200 Pa (left) and 1000 Pa (right) polyacrylamide gels.

Figure 16 displays the limitation we had contacting this experiment. It was not possible to perform the experiments ate the same distances from the tip. Beads embedded in the 200 Pa (n=10) polyacrylamide gel exhibited large displacement in proximity from the tip ending up either detaching from the gel or gel-bead was touching the tip of the electromagnet and ending up damaging the gel. For the 1000 Pa gel (n=9) greater distances from the tip didn't result in any movement of the embedded beads, measurable displacements were only observed at small distances, that was not optimal for the measuring displacement for the 200 Pa gel. The differences between the two experiments are expected as beads embedded in stiffer substrates will need larger magnetic forces to exhibit measurable displacements vice versa as we quantify them below.

The raw displacements of the superparamagnetic beads in the two experiments are displayed in **Figure 17**. No differences can be observed, with an average displacement of 2.15 μm for the 200 Pa hydrogel and. 2.40 μm for the 1000 Pa. Force-Distance differences are in place between the two experiments, thus creating misleading results. To counteract these dissimilarities the raw displacements where normalized using a simple rule of three:

ANTONIS MICHANIKOU

$$Nd = \frac{fd}{F}$$

Nd: Normalize Displacement

f: Constant Force

d: Raw displacement

F: Calibration Force from Force-distance curves

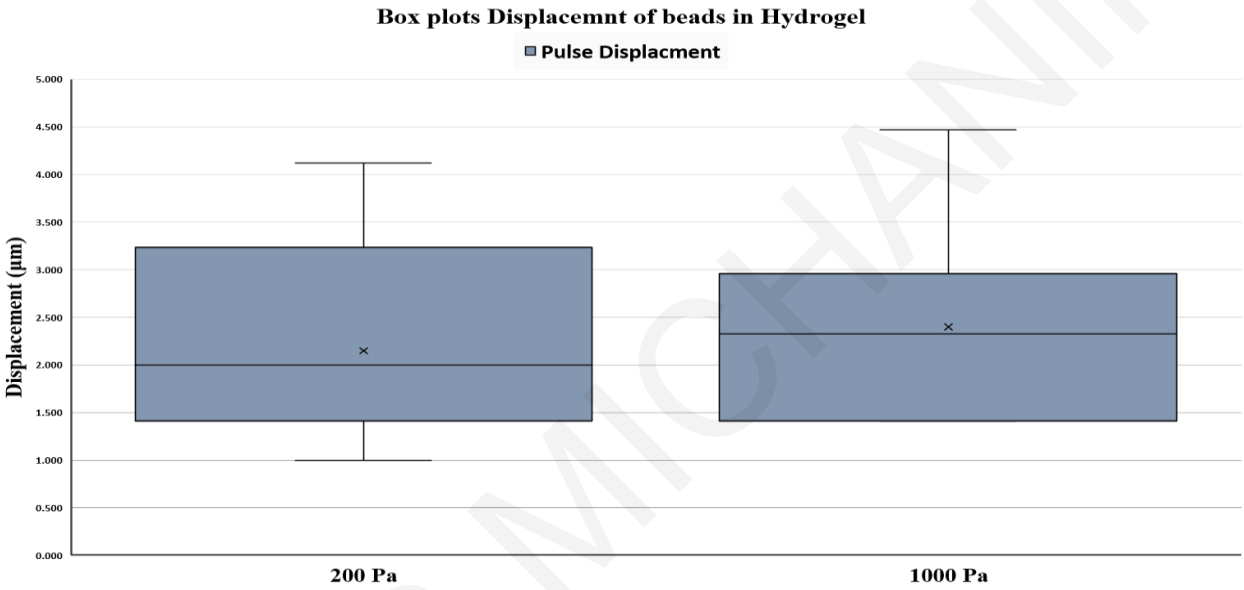

Figure 17: Raw Displacement (µm) of beads on 200 Pa and 1000 Pa polyacrylamide gels

After adjusting for force to distance differences, in the two experiments, the embedded beads in 1000 Pa polyacrylamide gel experience statistically significant mean (1.3 µm) ($p < .000$) smaller displacements than the softer 200 Pa hydrogel (4.9 µm). The box plots of the normalized displacements are shown in **Figure 18**. The results that are presented here indicate that when beads, that are embedded in polyacrylamide gels, are exposed to a uniform and equal magnetic field, will exhibit displacements relevant to the stiffness of the substrate in which they are embedded. As the elastic modulus increases, in polyacrylamide gels, the displacement decreases.

ANTONIS MICHANIKOU

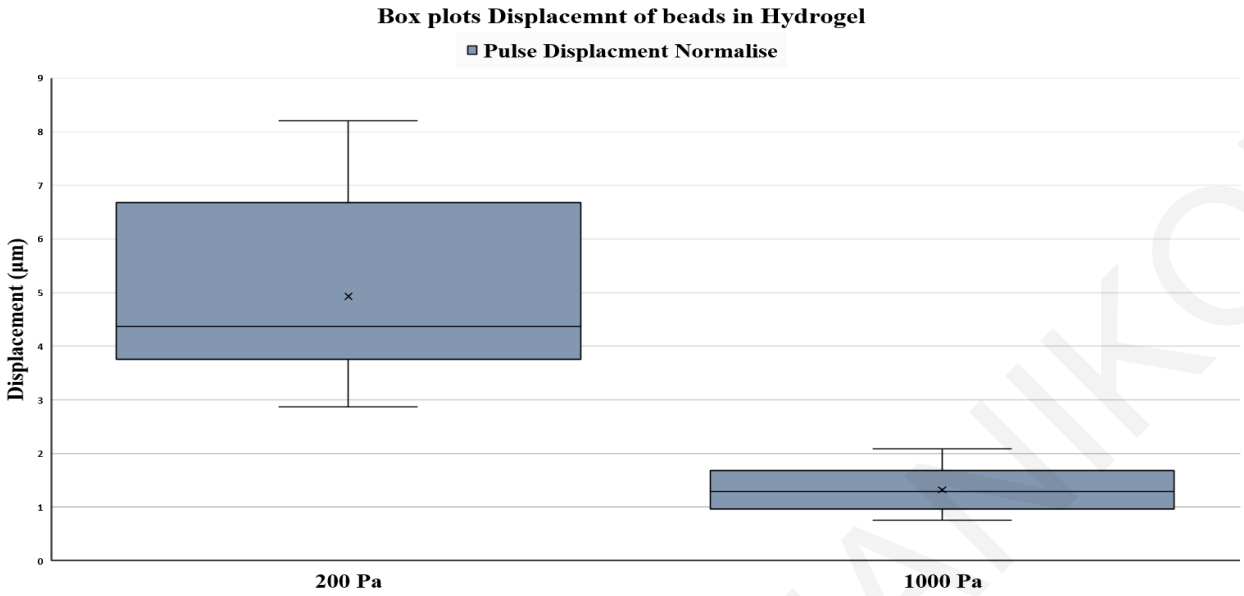

Figure 18: Normalized box plots displacements

Additionally, **Figure 19** represents the ratio of the recoil displacement and the initial pulse displacement, for both polyacrylamide gels. The mean displacement recovery of 200 Pa was 100%, and the beads in the 1000 Pa gel displayed a mean value of approximately 119%. Results that indicate that upon displacements due to the applied magnetic force the beads embedded in the polyacrylamide gels experience equal recoil displacements, thus returning to their original positions, confirming the elasticity of hydrogels.

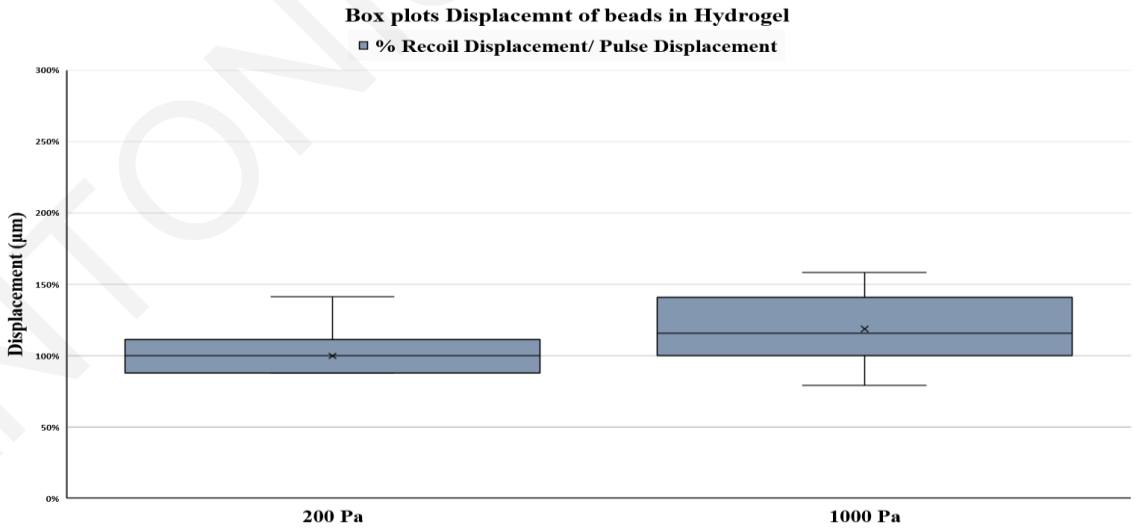

Figure 19: Ratio of recoil displacement and final displacement during the pulse.

ANTONIS MICHANIKOU

Initial experiments

Primary Cilia

Primary cilia are mechanosensory organelles and can transduce extracellular chemical and mechanical signals intracellularly, the aim of this initial project was to attach a superparamagnetic bead to the tip of the cilium and apply magnetic forces using our magnetic tweezer to bend the cilium and examine the intracellular calcium concentrations.
At first, we conducted initial experiments on MDCKs cells to confirm and calibrate the ciliogenesis process (**Figure 20**) as previous studies had implied (Bernabé-Rubio, Andrés et al. 2016).

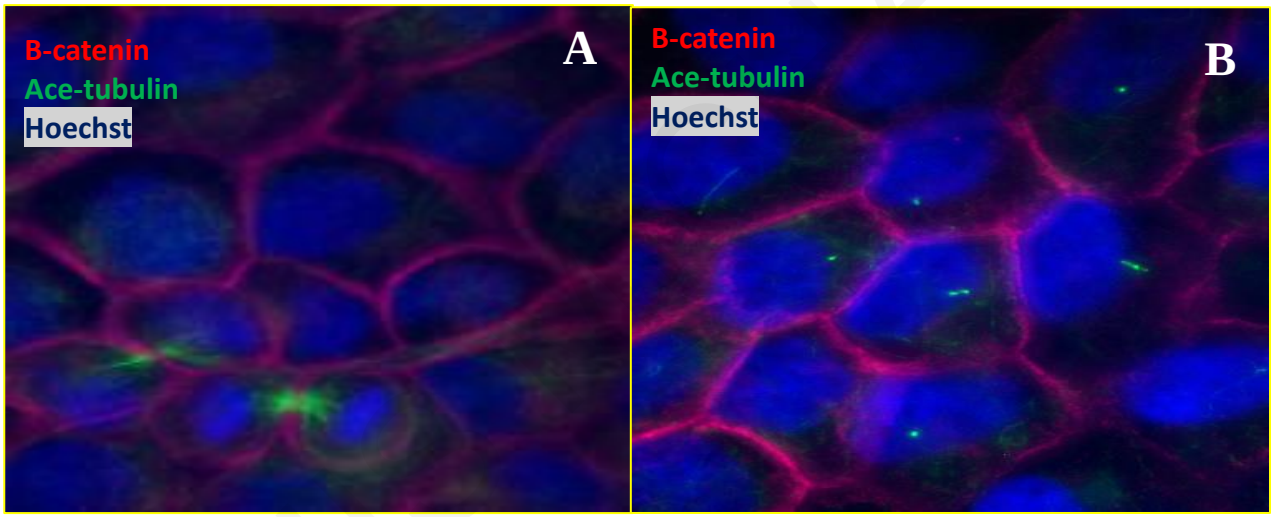

Figure 20: A) MDCKs cells with 10% FBS, B) MDCKs cells with 0.2% FBS

On Mdcks cells upon one day starvation with 0.2% FBS,upon fixations, they were stained against B-catenin and Ace-tubulin, we observed visible ciliogenesis (**Figure 20B**) as confirmed by Ace-tubulin. While (**Figure 20A**) with normal serum conditions this was not replicated.
For targeting the tip of the cilium we tested Proteintech(SMO ectodomain antibody),as the company stated it could target the Smoothened (Smo) ectodomain on MDCK cell line, and a Smo polyclonal antibody. Smo is expressed at the primary cilium and regulated by the Hedgehog pathway, one essential contribution of Smo is it role to the regulation of transcriptional factors belonging to the Gli family (Ruiz-Gómez, Molnar et al. 2007). In **Figure 21** MDCKs cells upon

24h starvation, they were fixed and stained against Arl13b and Smoothened using the Smo ectodomain antibody, and in **Figure 22** staining against Acetylated tubulin and Smo using the polyclonal antibody. The resulted IF didn't produce any visible expression of Smo in the MDCKs while we had visible ciliogenesis.

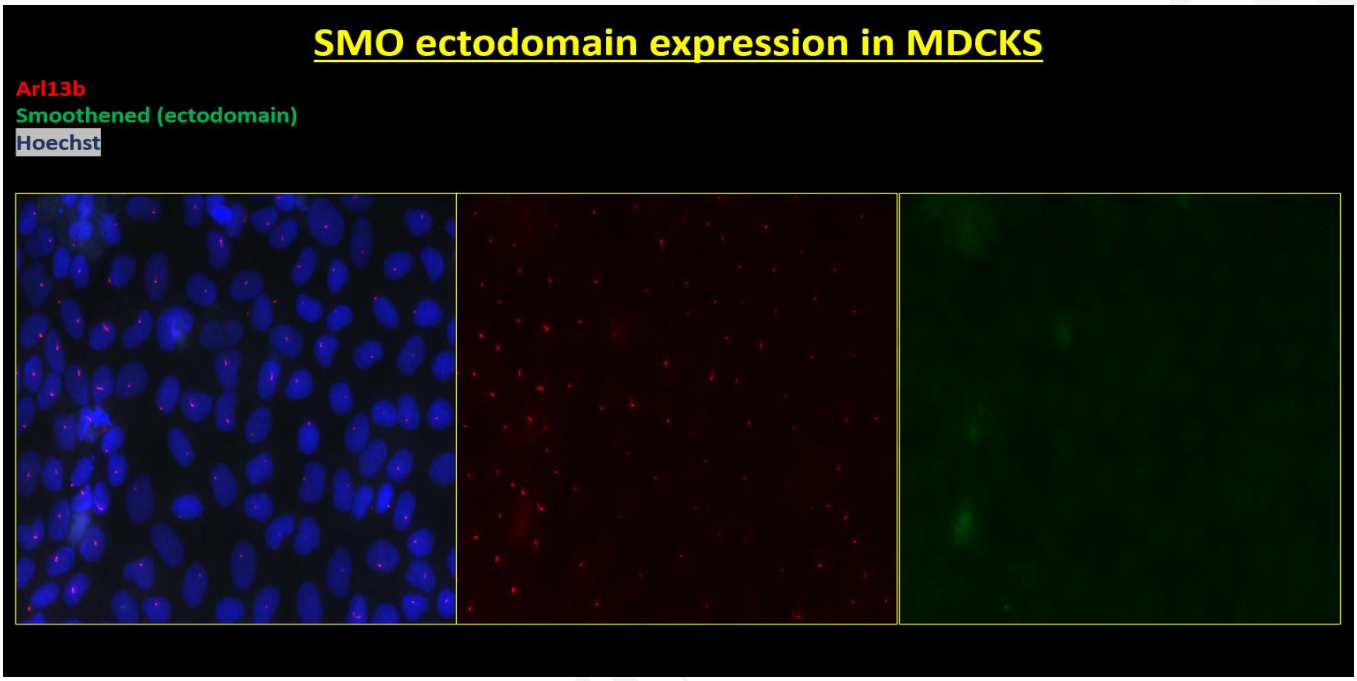

Figure 21: Expression of Smoothened using the Smo ectodomain antibody on MDCKs.

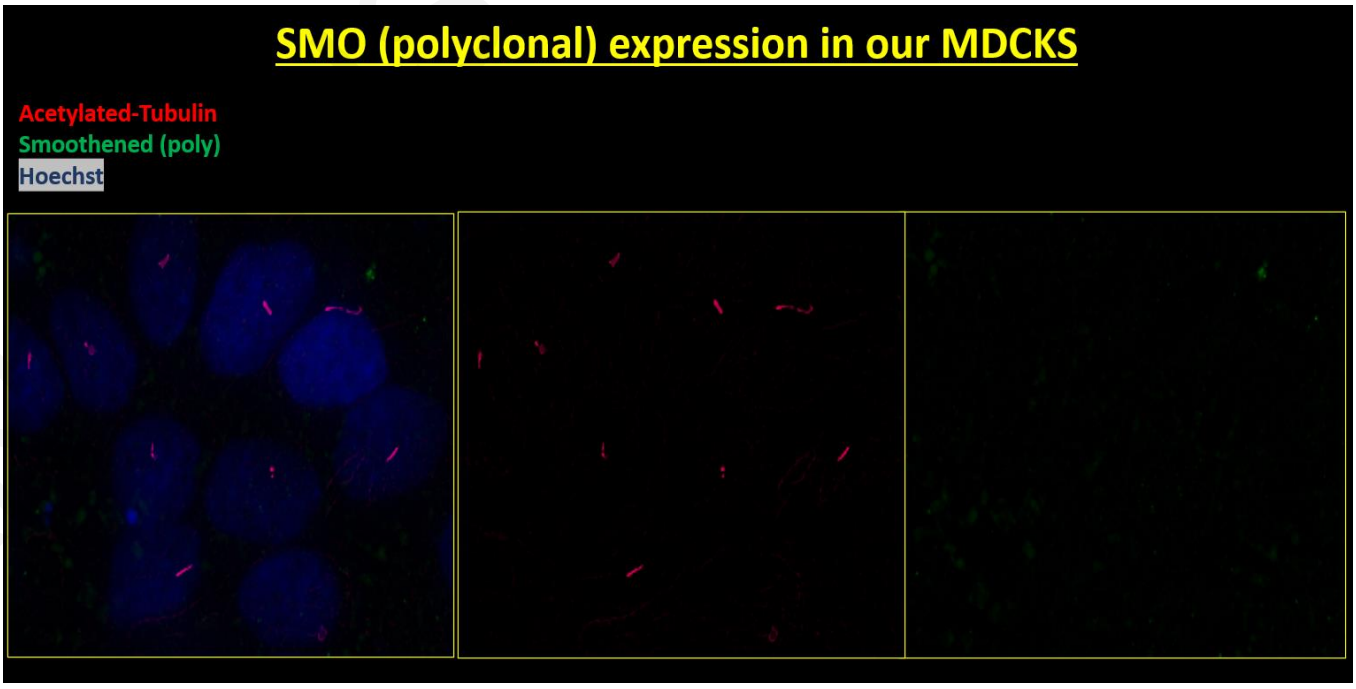

Figure 22: Expression of Smoothened using the Smo polyclonal antibody on MDCKs.

Moving forward we further seek to examine the bibliography, as previous study has stated partial inhibition of the Sonic Hedgehog (Shh) by Ptch1 blocks the localization of Smo to the primary cilium, activation of the Shh allows the entering of Smo and other proteins of the Gli family like Gli2 and Gli3 to enter the primary cilium (Han, Alvarez-Buylla 2010). To test this, we first needed to activate the Shh pathway, activation of the pathway can be done using SAG agonist, positive confirmation for the activation of the pathway and localization of targeted proteins to the primary cilium we used Gli3 antibody. With no compatible marker in our lab for Gli3 for MDCK cell line, we decided to test a different cell line.

We used IMCD-3 cell line, as is widely use and it is the most common cell line in studies for primary cilia (Sun, S., Fisher et al. 2019). IMCD-3 cells upon 24h starvation, they were fixed and stained against Acetylated tubulin, Gli3 and Smoothened using the Smo polyclonal antibody **Figure 23**. **Figure 24** IMCD-3 cells were stained against Arl13b, Gli3 and Smo using the ectodomain antibody.

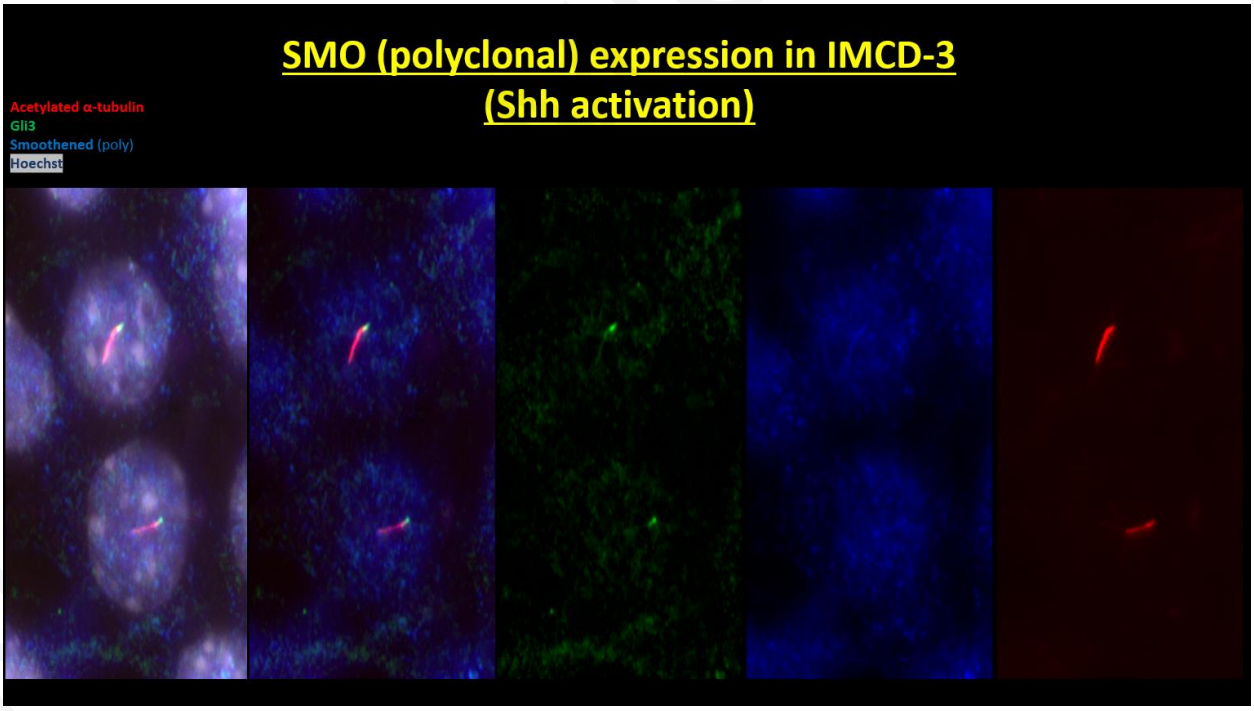

Figure 23: Expression of Smoothened using the Smo polyclonal antibody on IMCD-3 cells.

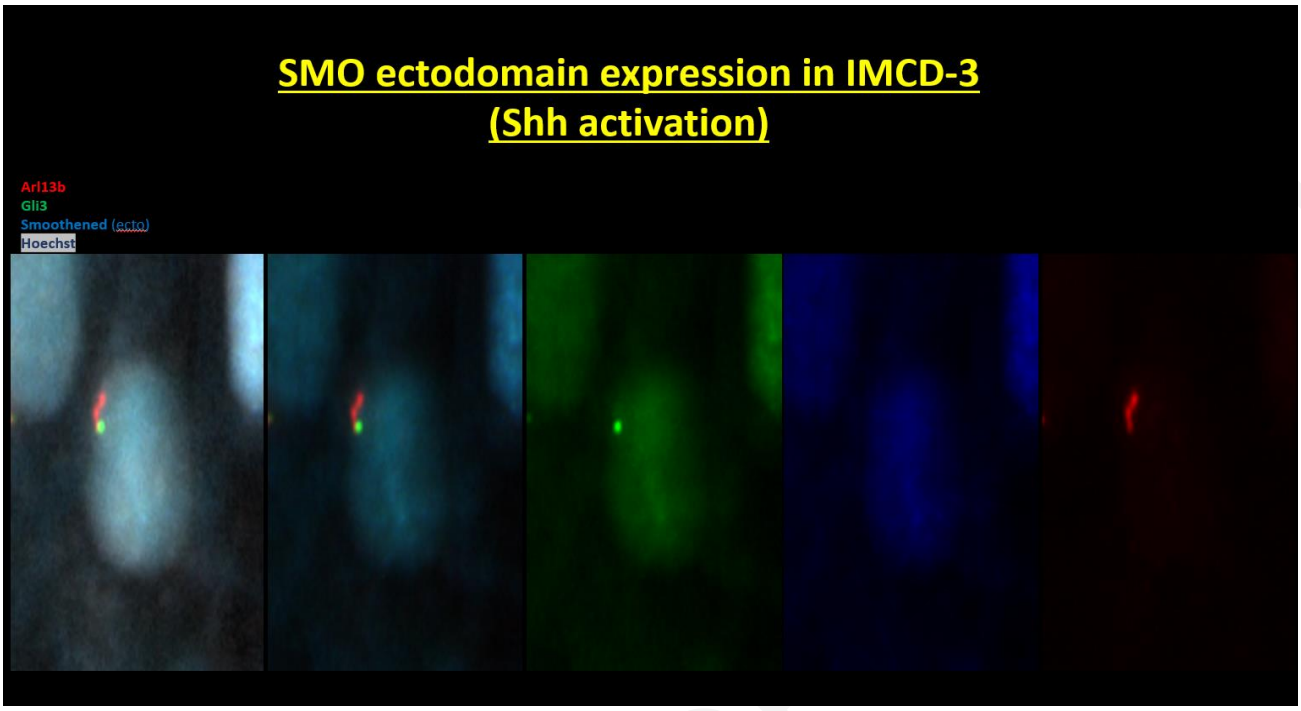

Figure 24: Expression of Smoothened using the Smo ectodomain antibody on IMCD-3 cells.

In both IFs activation of the pathway is confirmed by the translocation of the Gli3 to the tip of the primary cilium but in both IFs neither the polyclonal nor the ectodomain antibody is in the tip of the cilium as indicated by the Gli3.

We concluded that the antibody was not working as implied by the company and as no available antibody was found to target the tip of the cilium, we thus went on to address other biological questions using magnetic tweezers. These experiments need to be revisited once an appropriate antibody is obtained.

Using magnetic tweezers to promote tension driven integrin activation at ectopic adherens junctions.

We then proceed to explore the possibility of creating tension at ectopic adherens junctions (eAJs) to promote the mechanical activation of integrins. As previously reported AJs can regulate the spatial distribution and activation of integrins in the absence of extracellular matrix ligands (Hadjisavva, Anastasiou et al. 2022). We first conjugated the 4.5 superparamagnetic beads appropriately so than can interact with the cell cadherins on the cell membrane **Figure 25**

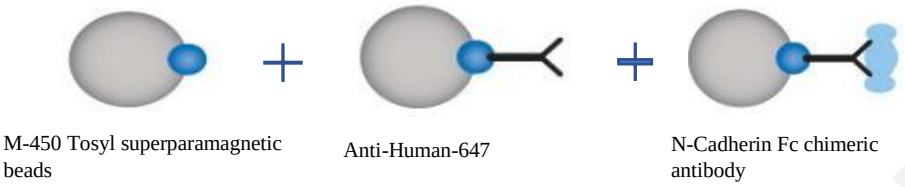

Figure 25: Schematic of the coating procedure for the M-450 Tosyl superparamagnetic beads.

N-Cadherin Fc (NFC) substrate was used to target cell membrane cadherins, for this purpose anti human 647 antibody was first coated with the beads and then with the NFC antibody. To test the functionality of the conjugated beads we incubated them with HeLa cells for 30 min before fixation and stained against N-cadherin and integrins **Figure 26**.

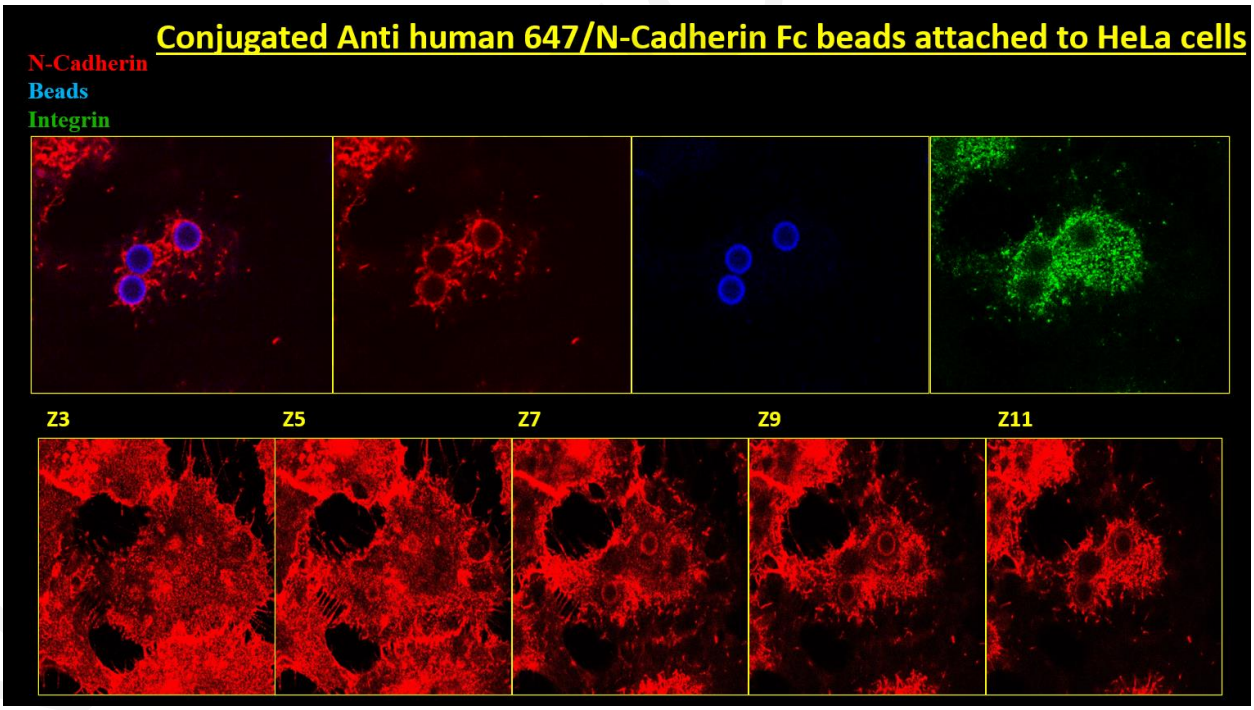

Figure 26: Schematic of the coating procedure for the M-450 Tosyl superparamagnetic beads.

While clustering of N-cadherin and integrin around the beads was confirmed from the IF the attachment of the beads to the cell was not optimal and as was scarce.

We then went on to optimize the attachment of the superparamagnetic beads using a ratio of anti-human 647 and anti-human antibodies for the first coating of the beads before using the NFC antibody (**Figure 27).**

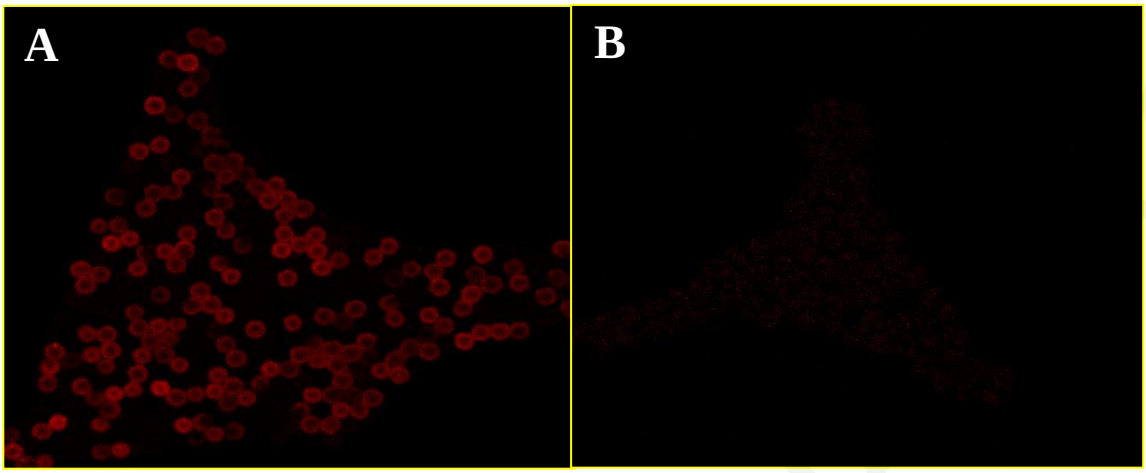

Figure 27: A) Beads with the ratio of Anti human 647 and anti-human.

B) M-450 Tosyl superparamagnetic beads.

Minimal fluorescence intensity for the M-450 beads was observed before coating with antibodies (**Figure 27B)** while after the successful conjugation with the antibodies we have an increase in fluorescence intensity (**Figure 27A)**.

These experiments show that magnetic beads can be used to address mechanosensing from AJ complexes and future work will be carried out to address cellular responses through AJ based mechanical stimulation.

Adhesion strength of coated superparamagnetic beads upon applied stress on HeLa cells

As shown above the custom MT system can apply quantifiable force on the tosyl activated beads. We thus wanted to use the MTs to address PM mechanosensing and changes in cellular mechanical properties upon mechanical stimulation. To do so we decided to explore integrin dependent and integrin independent mechanosensing at the PM and thus went on to generate Concanavalin A and Fibronectin covalently functionalized MBs using tosyl based chemistry. Concanavalin A (CONA) is a plant lectin that is purified from jack beans. CONA binds to the mannose residues of various glycoproteins and can thus be used to non-specifically link the

ANTONIS MICHAILOU

magnetic beads on the cell surface. Fibronectin (FN) on the other hand is a high-molecular weight glycoprotein of the extracellular matrix and a well characterized integrin ligand that allows integrin-based attachment of the MBs on the cell surface through its RGD peptide. To access the adhesion of different protein coated superparamagnetic beads on HeLa cells, 4.5 μm MBs Tosyl activated Dynabeads were conjugated with Fibronectin (FN) **(Figure 28**) and Concanavalin A(CONA). The two protein coated beads were incubated separately with HeLa cells on glass cover slips as described in the materials and methods section. Pulses were introduced ranging from 5-6 seconds to the beads and displacement and recoil displacement was measured using Fiji software. Before the introduction of a magnetic field, distance from the tip for each individual bead was measured. Beads that didn't exhibit recoil displacement where excluded. Measurable displacements of FN coated beads could only be observed from distances ranging from 16- 130 μm with a mean of 59 μm while CONA coated beads experienced displacements from a range of 37-192 μm with a mean of 110 μm (**Figure 29**), at smaller distances CONA beads at best were exhibiting no recoil displacement and, in most cases, complete detachment from cell membrane (**Figure 30**). The fact that CONA beads detach from the cell surface at lower force levels clearly shows that CONA leads to a weaker attachment of the beads on the cell surface compared to FN.

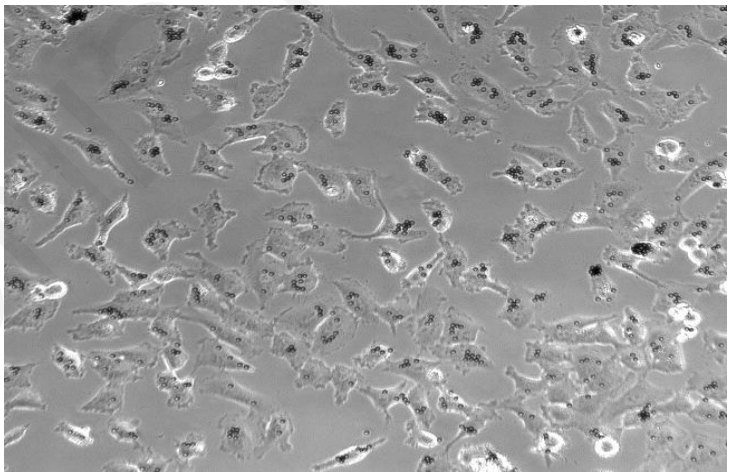

Figure 28: Fibronectin coated beads incubated with HeLa cells.

ANTONIS MICHANKOU

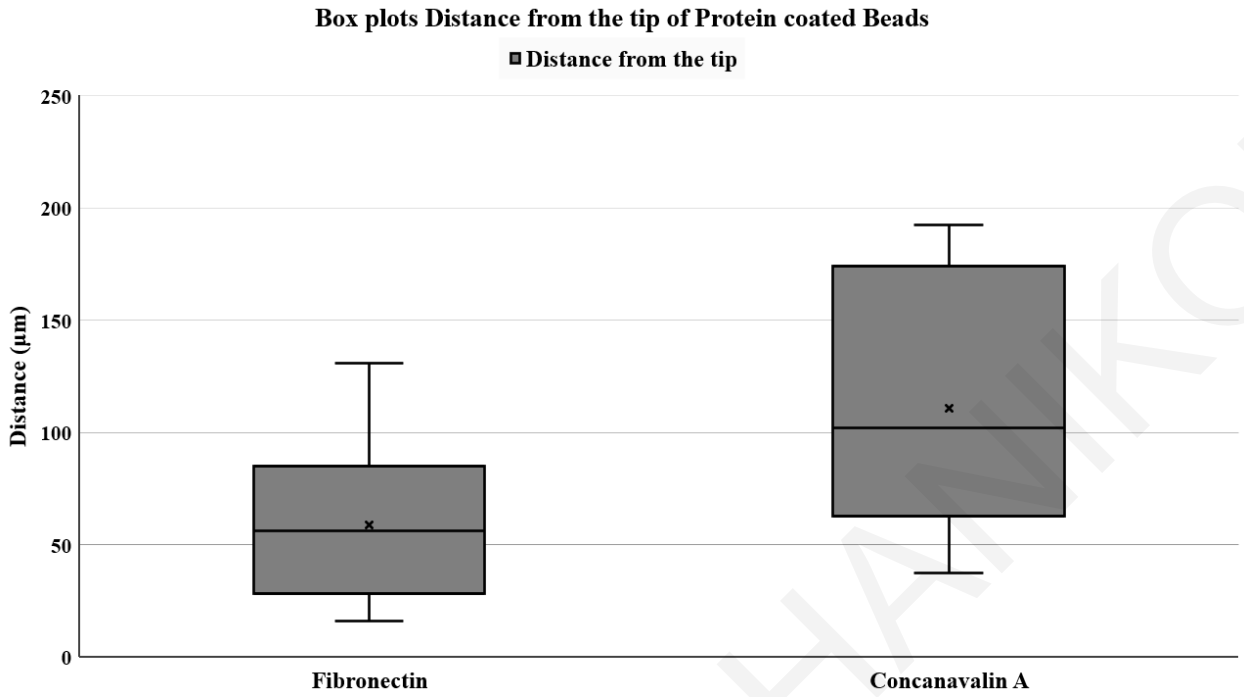

Figure 29: Distance from the magnetic tweezer between the two experiments.

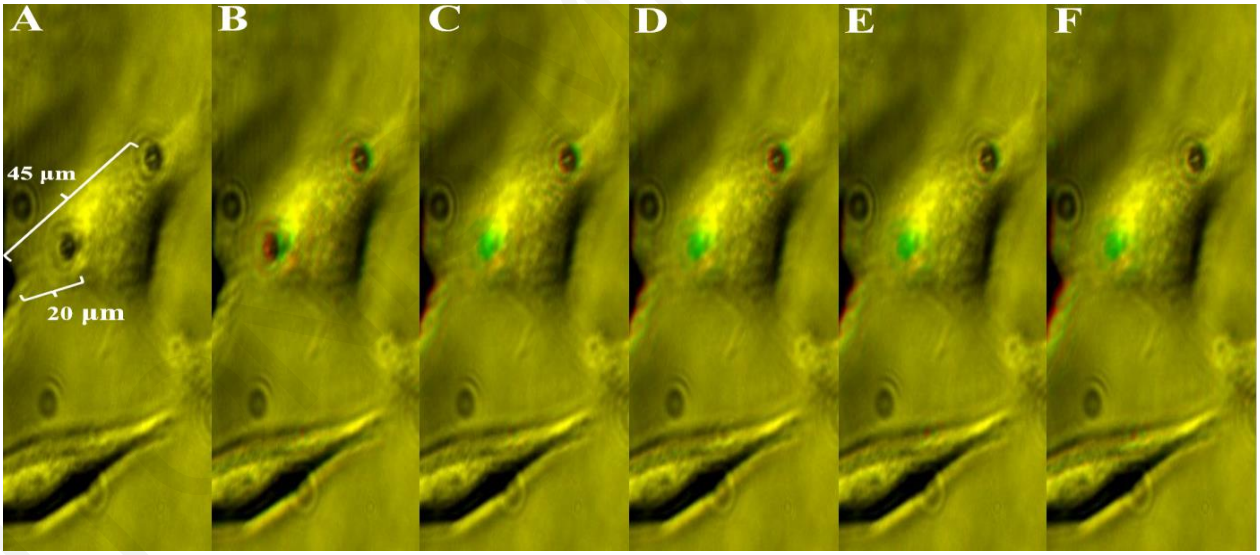

Figure 30: A) Before Pulse, B), C) and D) During the pulse, E) and F) After the pulse. Overlay of initial pulse(red) and each continuous frame(green). The coated CONA bead closest to the tip experience large displacement during the first 2 seconds of the magnetic pulse then it detaches from the cell. While a bead 45 µm away from the magnetic tweezer experience a smaller displacement during the pulse and returns to its original position after the pulse.

To access the impact of the distance from the tip to the resulting displacement of the beads, regression analysis was performed, **Figure 31**. Statistically significant results were found for CONA conjugated beads, (R^2 = .35, F (1, 10) = 5.50, p =.04), and for the FN coated beads (R^2 = .61, F(1, 11) = 16.85, p = .001) Table 2.

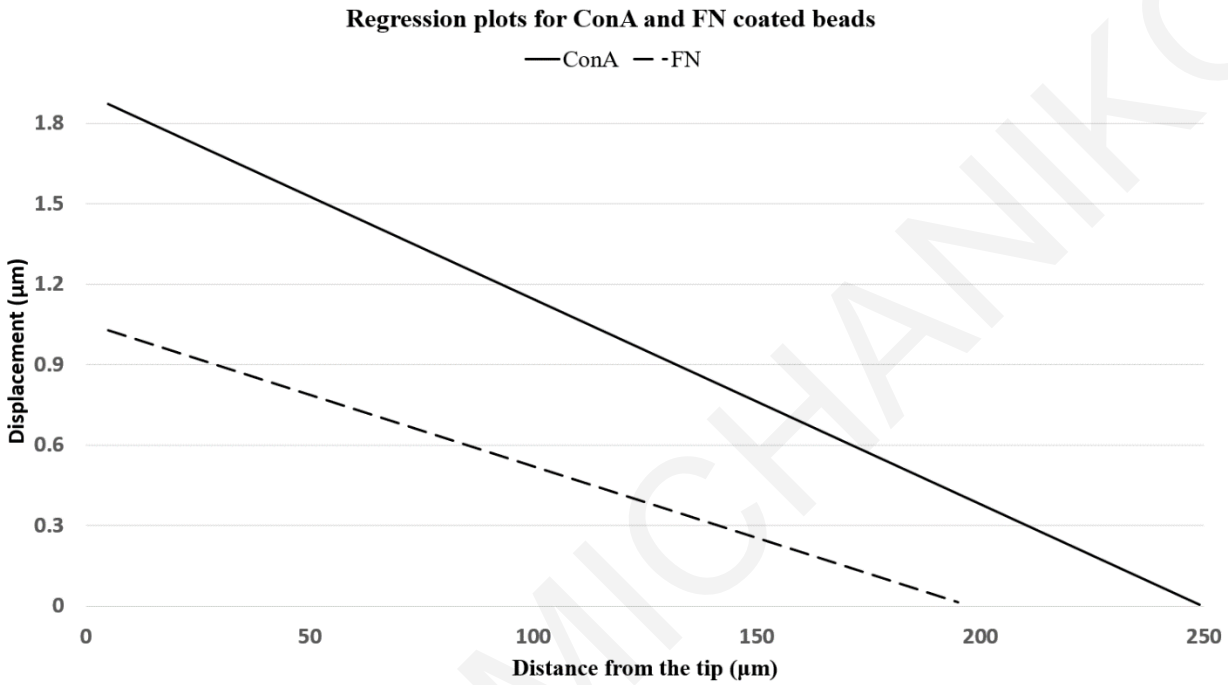

Figure 31: Linear regression plots based on the results of Table 2.

Experiment	Current	b0	p-value(b0)	b1	p-value(b1)
CONA Beads	3000 mA	1.91	p < .000	-0.008	p = .04
FN Beads	3000 mA	1.06	p < .000	-0.005	p < .000

Table 2: b0 and b1 coefficients with their calculated p-values for each experiment.

Fibronectin is known to bind integrins, Concanavalin A shows no specificity, The CONA beads are experiencing greater displacements than the FN beads and at a longer distance than the Fibronectin coated beads. This is likely a result of the fact that CONA bead displacement can be accomplished by simple PM deformation and thus there is only one source of resistance on the bead while Fn bead displacement requires a combination of PM deformation and actomyosin

ANTONIS MICHANIKOU

elongation. This could also be an indication of the attachment of each bead, additionally the measurements of the CONA beads are indicating increasing variance between the measurements, comparing them to the FN beads, with an $R^2 = 0.35$ and $R^2 = 0.61$, respectively, which can also used as an indication for the specificity of each bead.

Effect of mechanical stress on Hela cells through integrin receptors during magnetic pulses

The above data show that using FN and CONA coated beads in conjunction with the MT we can directly apply mech stimulation on the cell PM. The two beads would be expected to stimulate the cell through different mechanisms. FN beads would be expected to result in integrin-based responses while responses to CONA bead mech stim could potentially result in responses based on other PM mechanosensors such as mechanically gated channels, curvature-sensing proteins and even responses elicited by transmembrane protein conformational adaptation to changes in bilayer thickness via increased PM tension. In order to assess the impact of direct stimulation of the cell PM via integrin based and CONA based adhesion on the mechanical properties of the cell was determined through the displacements of the two different coated type of beads was assessed through five sequentially patterns of a magnetic Pulse and a relaxation phase lasting 5-6 seconds respectively. Additionally, Cytochalasin D and Rho Kinase Inhibitor were introduced in different cover slips to further assess the effect of these inhibitors on the displacement of the beads in each case, thus creating 6 different scenarios:

1) FN-beads with no treatment with a drug
2) FN- beads with the addition of Cytochalasin D (CYTO)
3) FN-beads with treatment of Rho kinase inhibitor (ROCK)
4) CONA-beads with no treatment with a drug
5) FN- beads with the addition of Cytochalasin D (CYTO)
6) FN-beads with treatment of Rho kinase inhibitor (ROCK)

The CYTO and ROCK inhibitor treatments would allow us to address the roles of the actin cytoskeleton and cell contractility respectively on cellular responses to mechanical stimulation while at the same time provide information (through their impact on the first displacement and recoil) on their contribution to the PM mechanical properties. To counteract the differences in

ANTONIS MICHANIKOU

distance from the tip and by extension different forces applied to FN and CONA conjugated beads, displacements (**Figure 32**) and recoil were normalized in the same manner as the polyacrylamide gels. First we performed one-way ANOVA test in all sets of displacements FN-NT, FN-CYTO, FN-ROCK, CONA-NT, CONA-CYTO and CONA-ROCK, **Table 3**.

Statistically important results were identified only in FN-NT displacements ($F(4, 36) = [6.778]$, $p<.05$). Result that indicates that between the set of the 5 normalize displacements for the FN-NT beads they are statistically important differences, while the mean values of the displacements (**Figure 32,Table 3)** for the FN-NT beads are displaying a gradual decrease in the displacements with the progression of the pulses we furthered seek to access the significance of this result ,we conducted pair comparisons using Welch's t-test between the first normalize pulse displacement and fifth normalize pulse displacement that the beads experienced, as well as second pulse and fifth pulse comparisons. Comparisons for the other experiments were done also, as some experiment, while not statistically significant, experience marginal differences as indicated by the p values of the ANOVA test **Table 3**.

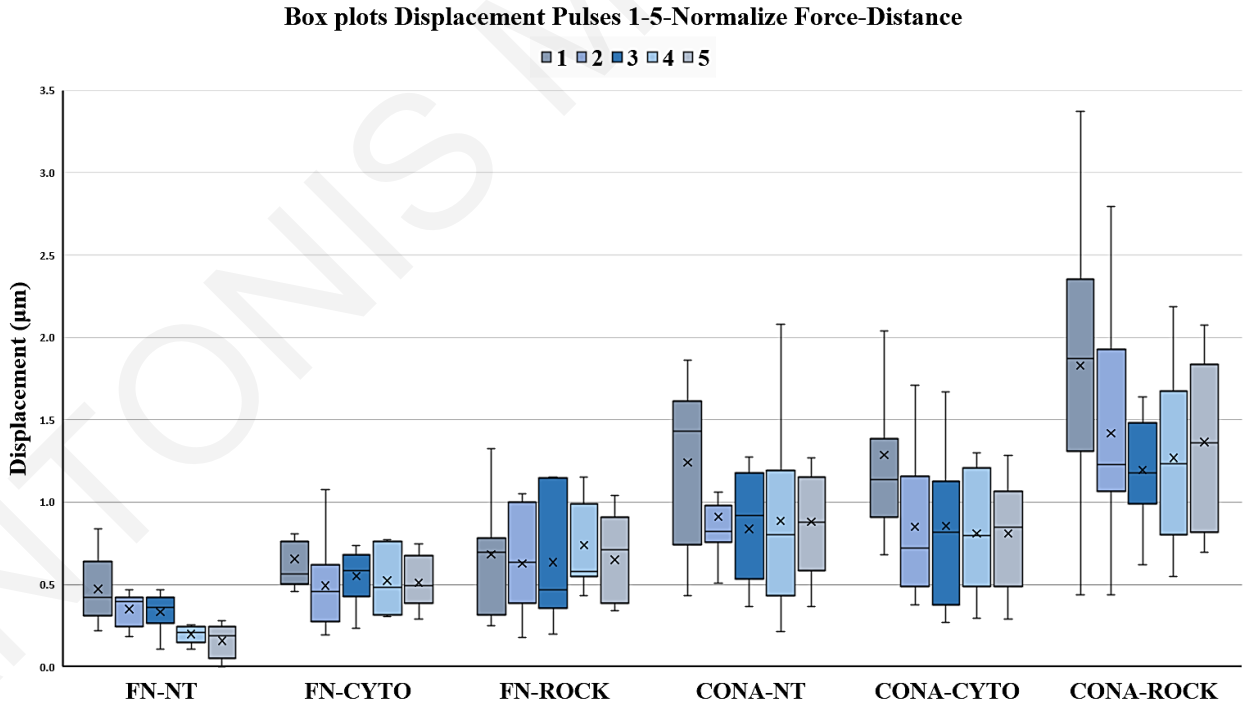

ANTONIS MICHALIKOU

Figure 32: Displacements of 4.5 superparamagnetic beads coated with FN and CONA with and without Cytochalasin D and Rho Kinase Inhibitor.

Experiment displacement	Pulse 1 (μm) mean	Pulse 2 (μm) mean	Pulse 3 (μm) mean	Pulse 4 (μm) mean	Pulse 5 (μm) mean	n	F	p-value
FN-NT	0.47	0.35	0.33	0.20	0.16	36	6.78	0.000
FN-CYTO	0.66	0.49	0.55	0.52	0.51	35	0.70	0.597
FN-ROCK	0.68	0.63	0.64	0.74	0.65	30	0.14	0.968
CONA-NT	1.24	0.91	0.84	0.89	0.88	50	1.81	0.142
CONA-CYTO	1.29	0.85	0.86	0.81	0.81	50	2.11	0.093
CONA-ROCK	1.83	1.42	1.19	1.27	1.36	45	1.75	0.155

Table 3: Results from one-way ANOVA test performed to the 5-set of normalize displacements for each experiment.

For the fibronectin conjugated beads (**Figure 33**) statistically significant differences were found only within the group that we didn't add an inhibitor (FN-NT), with a $p<.05$ between the pair 1^{st} - 5^{th} Pulse and 2^{nd} - 5^{th} ($p<.05$) . Furthermore, for the Concanavalin A beads (**Figure 34**) statistically significant differences were observed only between 1^{st} - 5^{th} Pulse in the CONA-CYTO ($p<.05$) but the effect didn't observe when comparing the 2^{nd} - 5^{th} ($p=0.82$). Marginal differences were observed among the 1^{st} - 5^{th} Pulse in the CONA-NT ($p=.053$) put as for the CONA-CYTO beads the effect didn't continue 2^{nd} - 5^{th} ($p=0.81$).

ANTONIS MICHANKOU

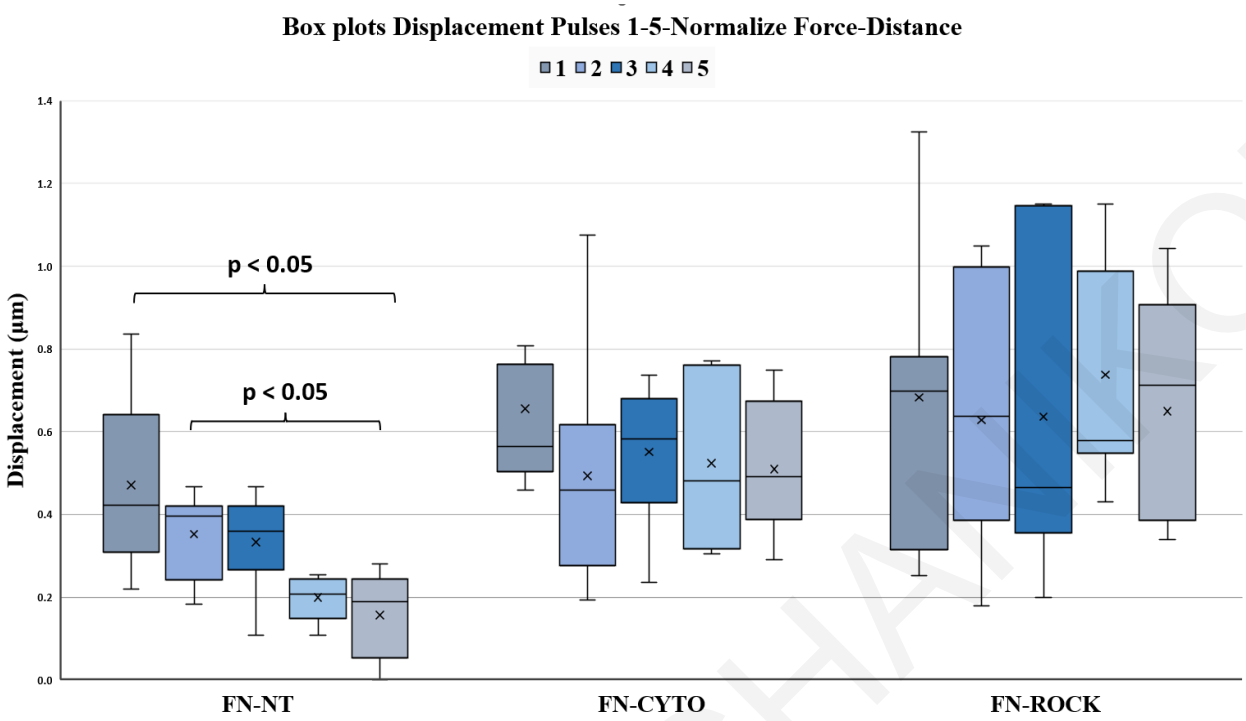

Figure 33: Displacements of 4.5 superparamagnetic beads coated with fibronectin with and without Cytochalasin D and Rho Kinase Inhibitor.

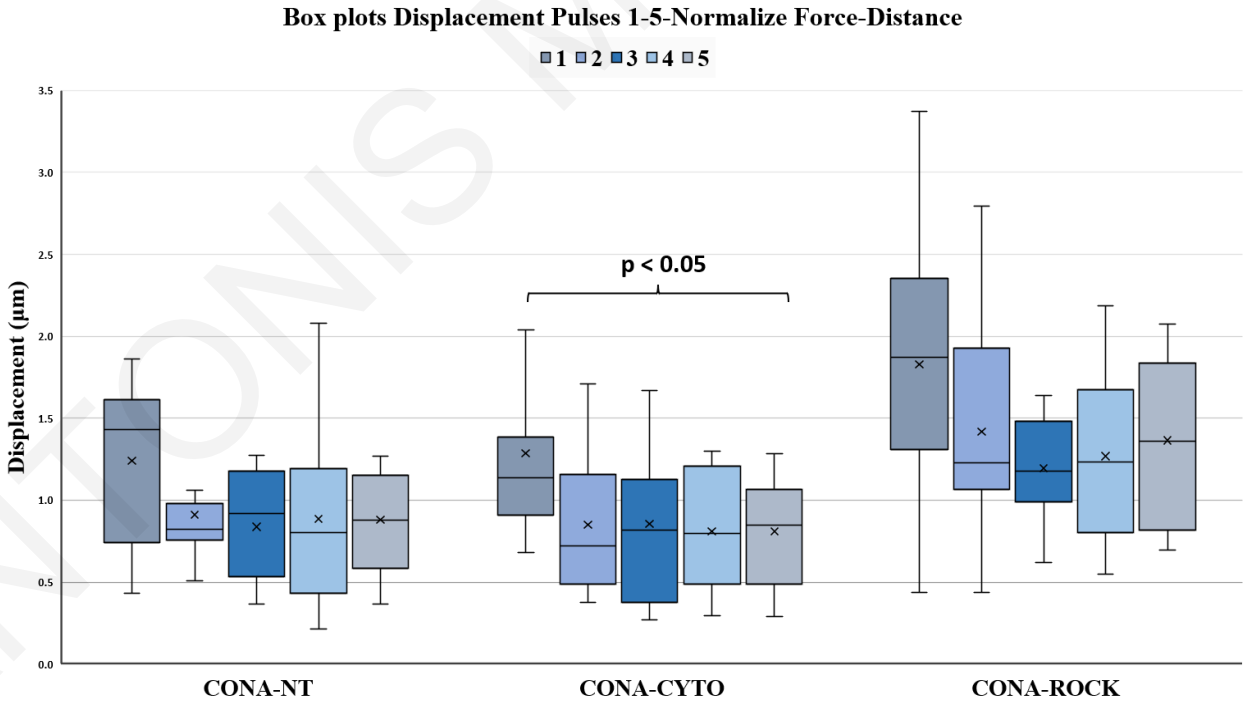

Figure 34: Displacements of 4.5 superparamagnetic beads coated with Concanavalin A with and without Cytochalasin D and Rho Kinase Inhibitor.

ANTONIS MICHAILOU

The gradual decrease that the beads experience in the FN-NT group is statistically significant between the first and fifth pulse and the effect is also observable between the second pulse and fifth, a result that didn't replicate between the other 5 experiments. Furthermore, significant, or marginal differences were observed only between the comparison of the 1st with the 5th Pulse. The results indicate that the beads in the experiments experience some differences either marginal or significant, but the effect is not carried out throughout the pulses, except for the FN-NT beads, to better understand the effect of this difference, comparisons within all pulses was then carried out to assess the similarities and differences between displacement pulses in each experiment. Additional differences were found within the FN-NT beads, $1^{st} – 4^{th}$ pulse ($p<.05$), $2^{nd} – 4^{th}$ ($p<.05$), $2^{nd} – 5^{th}$ ($p<.05$),$3^{rd} – 4^{th}$ ($p<.05$), $3^{rd} – 5^{th}$ ($p<.05$). For the CONA beads statistically significant differences were found at CONA-NT ($1^{st} – 3^{rd}$ Pulse ,$p<.05$)and CONA ROCK beads($1^{st} – 3^{rd}$ Pulse ,$p<.05$). No statistically significant differences were found between any other comparison. Interestingly, no differences were observed across all experiments between the pairs of $2^{nd} – 3^{rd}$ Pulse and $4^{th} – 5^{th}$ Pulse. The two pulses were then combined, and the mean values of the results are displayed in **Figure 35**, were B and C represent the combined displacements of $2^{nd} – 3^{rd}$ Pulse and $4^{th} – 5^{th}$ Pulse respectively, and A is the initial displacement during the first pulse. A decrease of 46% ($p<.05$) was observed in the comparison of B and C for the FN-NT coated beads with an overall decrease of 61% ($p<.05$) comparing A and C (**Figure 35(1)**), no statistically significant results was found for FN-CYTO (A-C, -21%, $p=.19$) or FN-ROCK beads. For the CONA-NT beads an equal decrease of -29% ($p<.05$) between A-B and A-C ($p=.055$) was observed. CONA-ROCK beads exhibit an A-B, -29% ($p=.09$) decrease and A-C, -28% ($p=.09$) but is not statistically significant, while CONA-CYTO beads results showed an A-C, -37% ($p<.05$) decrease (**Figure 35(2)**). These results indicate that both CONA-NT and FN-NT experience a decrease in the displacements between the A and B, but the magnitude is not equal. The non-specific binding of Concanavalin A is subject to cortical stiffness through other mechanisms, like intermediate filaments or mechanosensing channels with close relationship with the phospholipid membrane (Xue, Cox et al. 2020) that stiffening the membrane upon applied stress. The effect though is not observable as the pulses continue and reaches a plateau immediately after the initial displacement, a result that is replicated in both CONA-CYTO beads and CONA-ROCK beads.

ANTONIS MICHANIKOU

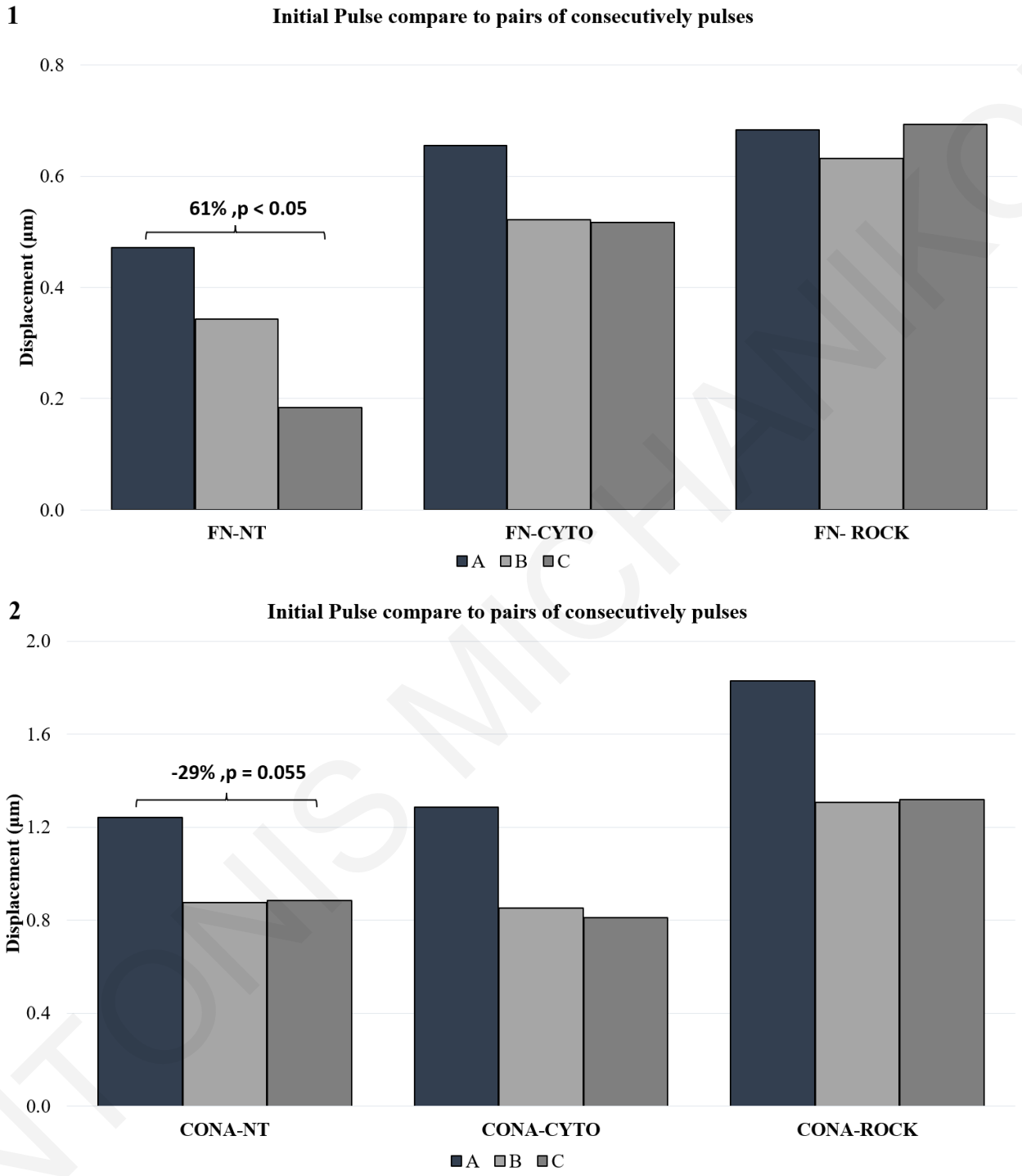

Figure 35: 1) FN conjugated beads and 2) CONA conjugated beads. A is the mean displacement for the initial first pulse, B and C the pair of 2^{nd} – 3^{rd} pulse and 4^{th} – 5^{th} correspondingly.

ANTONIS MICHAILIKOU

On the other hand, the specific binding of fibronectin to integrins on the plasma membrane is not only subjected to cortical stiffness. The FN-NT beads are displaying a more crucial decrease of -46% from A to B that is gradient as the pulses continue reaching a -61% decrease. Upon treatment with Cytochalasin D, that affects the polymerization of actin, the FN-CYTO beads, while not statistically significant, are displaying a decrease of -21%, and then is reaching a plateau, in the same manner as CONA-NT, CONA-CYTO and CONA-ROCK beads. When FN beads are introduced with the ROCK inhibitor that has bidirectional effect of inhibiting the polymerization of actin and the contractile force of actomyosin no significant or marginal effects can be observed in both comparisons between A-C and A-B. The above results obtain from the experiments with fibronectin coated beads indicated that the stiffening of the cell via Integrin dependent mechanism is entirely regulated through the actin cytoskeleton and the actomyosin contractility, confirmed by the treatment of the cells with different inhibitors that affect both actomyosin and the actin cytoskeleton (Wakatsuki, Schwab et al. 2001, Samuel, Lopez et al. 2011).

Furthermore, no statistical differences were identified between pair comparisons of the initial pulse A of FN-NT, FN-CYTO, FN-ROCK. Same results were observed between the initial pulses of the three experiments of the CONA beads **Table 4**.

1st Pulse comparison	**p-value**
FN-NT and FN-CYTO	0.11
FN-NT and FN-ROCK	0.19
FN-CYTO and FN ROCK	0.87
CONA-NT and CONA-CYTO	0.85
CONA-NT and CONA-ROCK	0.07
CONA-CYTO and CONA-ROCK	0.11

Table 4: Pair comparisons between initial Pulses

While there are statistical marginal differences between the FN-NT beads with comparisons with the FN-CYTO and FN-ROCK, they are not significant, this is maybe due to the high variance between the experiments and the small sample size. One should expect with the inhibition with CYTO and ROCK the displacements should increase, as you further disrupt the actin cytoskeleton, while this is represented at the mean displacements of FN-NT (0.47 μm) , FN-CYTO (0.66 μm) and FN-ROCK (0.68 μm) due to the limitation of the sample size and the

ANTONIS MICHANKOU

variance is not statistically significant, but nevertheless provides a logical outcome as with the treatment of drugs that affect the actin cytoskeleton we have an increase in the initial displacement. For the CONA beads that their displacements are subjected to overall cell stiffness and not entirely on cortical stiffness the same increase in mean was observed only for the comparison between CONA-NT and CONA-ROCK (1.83), (p=0.07), an increase of the magnitude of 48% was observed but is not statistically significant, again due possibly to the limitations of our sample size and variance displacement. In contrast a mean increase was not observed when comparing the initial displacement between CONA-NT (1.24 μm) and CONA-CYTO (1.29 μm),(p=0.85),one possible explanation is that the Cytochalasin treatment of the CONA beads was not successful and we can't observe any differences in the initial displacements.

Before concluding on the above results, we set to also examine the recoil displacements that we obtain from the experiments, in **Figure 14** are the box plots for the normalize recoil displacements of each experiment. As for the normalize displacements that was shown before (**Figure 36**), we conducted ANOVA test in each of the sets of pulses the results are presented in **Table 5**.

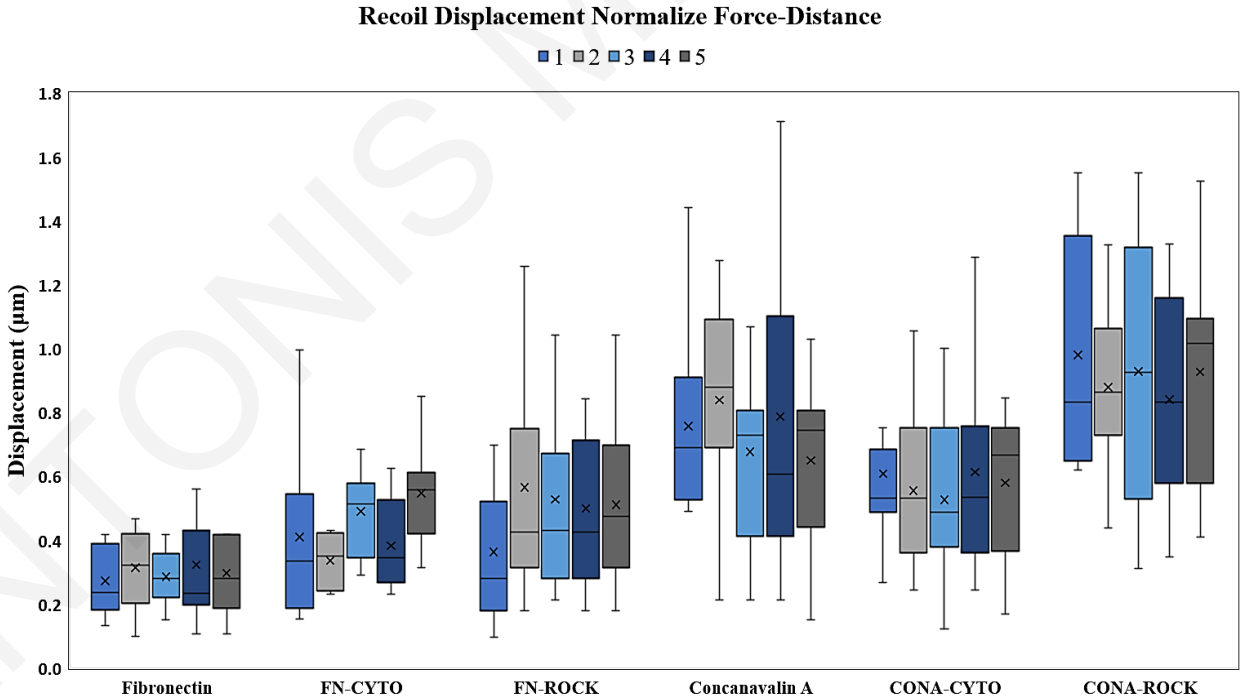

Figure 36: Recoil displacements of 4.5 superparamagnetic beads coated with FN and CONA with and without Cytochalasin D and Rho Kinase Inhibitor.

ANTONIS MICHANKOU

Experiment Recoil displacement	Pulse 1 (μm) mean	Pulse 2 (μm) mean	Pulse 3 (μm) mean	Pulse 4 (μm) mean	Pulse 5 (μm) mean	n	F	p-value
FN-NT	0.27	0.31	0.29	0.32	0.30	36	0.18	0.950
FN-CYTO	0.41	0.34	0.49	0.38	0.55	35	1.93	0.128
FN-ROCK	0.36	0.56	0.53	0.50	0.51	30	0.51	0.727
CONA-NT	0.76	0.84	0.68	0.79	0.65	50	0.63	0.644
CONA-CYTO	0.61	0.55	0.53	0.61	0.58	50	0.19	0.941
CONA-ROCK	0.98	0.88	0.93	0.84	0.93	45	0.25	0.910

Table 5: Results from one-way ANOVA test performed to the 5-set of normalize recoil displacements for each experiment.

No statistically significant results were obtained a marginal difference seems to be in place in the FN-CYTO experiment with a p value= 0.128 as the box plots showcased a slight increase in the recoil displacements as the pulses continue, and indeed within comparisons of the recoil pulses for the FN-CYTO statistically significant increase was observed between the recoil displacement of the second pulse and fifth pulse ($p<0.000$) with an increase of 63% , this is maybe due to the fact that the bead in this pulse exhibit large displacement from the magnetic pulse and thus increase its recoil displacement , but the ANOVA test for the displacements that was shown before Table 3, didn't show any differences between the displacements of the pulses and neither the individual comparisons that were done after. The notion that due to the decrease of actin polymerization there is an increase in cortical tension thus more myosin molecules can bind per filament was reported before (Bergert, Chandradoss et al. 2012, Blanchoin, Boujemaa-Paterski et al. 2014). Based on our results here we cannot address that.

Additionally, a more graphical representation of the connection of displacement and recoil is shown in **Figure 37**, that displays the ratio of recoil/displacement of each individual bead thought the pulses. One way ANOVA test between the first ratio of the Pulse-relaxation for all

ANTONIS MICHANIKOU

experiments showcased no differences (F (5, 50) = [0.45], p = 0.81) and ratios between 51% - 64%. That indicates that the displacement of the first pulse across all experiments is correlated with the recoil displacement in an equal manner. As shown from the analysis above for the displacements and recoil, the ratio provides a more graphical representation of what is happening during each pulse and the relaxations phase.

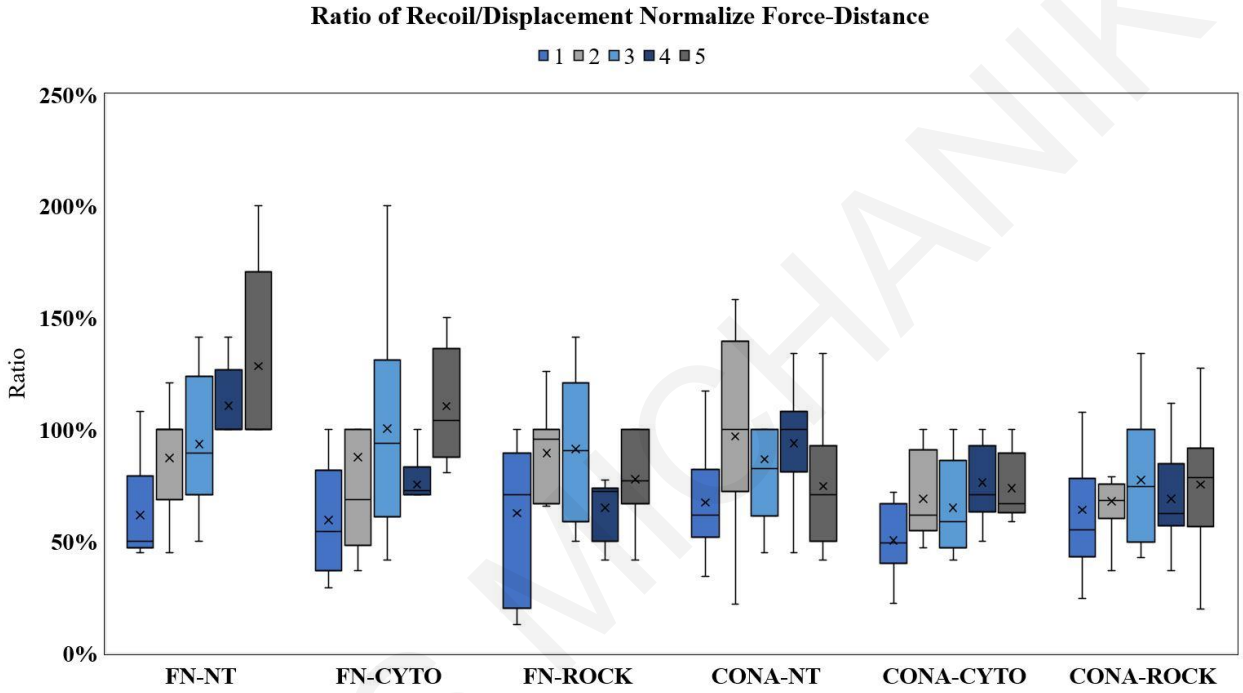

Figure 37: Ratio Displacement/recoil box plots for all the experiments.

For the FN beads the increasing ratio is observed only in FN-NT and FN-CYTO but not in the FN-ROCK, inhibition of myosin influences the contractility response of the cell, while treatment with cytochalasin is not, as is affecting actin polymerization not myosin-based contractility. While for the CONA beads the increase ratio effect is not observed as neither displacement or recoil displacements show any decrease or increase as the pulses continue, maintaining the plasticity effects of the membrane throughout the pulses.

Finally, to construct the complete movement of the beads throughout the pulses and give us a clearer understanding on how the beads were reacting to the continuous magnetic forces and

ANTONIS MICHANIKOU

relaxation phases we visualize the 6 profiles of the magnetic beads through the pulses using the mean values of normalize displacements and recoil **Table 6**.

Mean Displacement(μm)	FN-NT (n=14)	FN-CYTO (n=13)	FN-ROCK (n=11)	CONA-NT (n=14)	CONA-CYTO (n=12)	CONA-ROCK (n=11)
1st Pulse	0.55	0.66	0.79	0.95	1.33	1.58
Recoil	0.33	0.40	0.52	0.62	0.63	0.81
2nd Pulse	0.36	0.49	0.76	0.75	0.89	1.14
Recoil	0.33	0.34	0.68	0.60	0.55	0.78
3rd Pulse	0.33	0.59	0.75	0.60	0.77	1.07
Recoil	0.34	0.53	0.65	0.47	0.51	0.81
4th Pulse	0.22	0.56	0.84	0.61	0.80	1.08
Recoil	0.31	0.49	0.51	0.62	0.59	0.74
5th Pulse	0.17	0.54	0.78	0.73	0.80	1.14
Recoil	0.33	0.58	0.61	0.59	0.68	0.79

Table 4: Mean raw displacements and recoil

In **Figure 38** is the visualization of both the displacements and recoil through the 5 pulses. One important aspect of this representation is that the beads are exhibiting smaller recoil displacements in each pulse vs the displacements upon applied magnetic force and thus do not return to their original position and this is observed in all the experiments. This is expected, as upon removal of the mechanical load the return of the beads is incomplete either from viscoelastic effect that follow a power law time response (more relaxation time to return to its original position), or due to plasticity effects of the cell itself (Bonakdar, Gerum et al. 2016).

ANTONIS MICHANIKOU

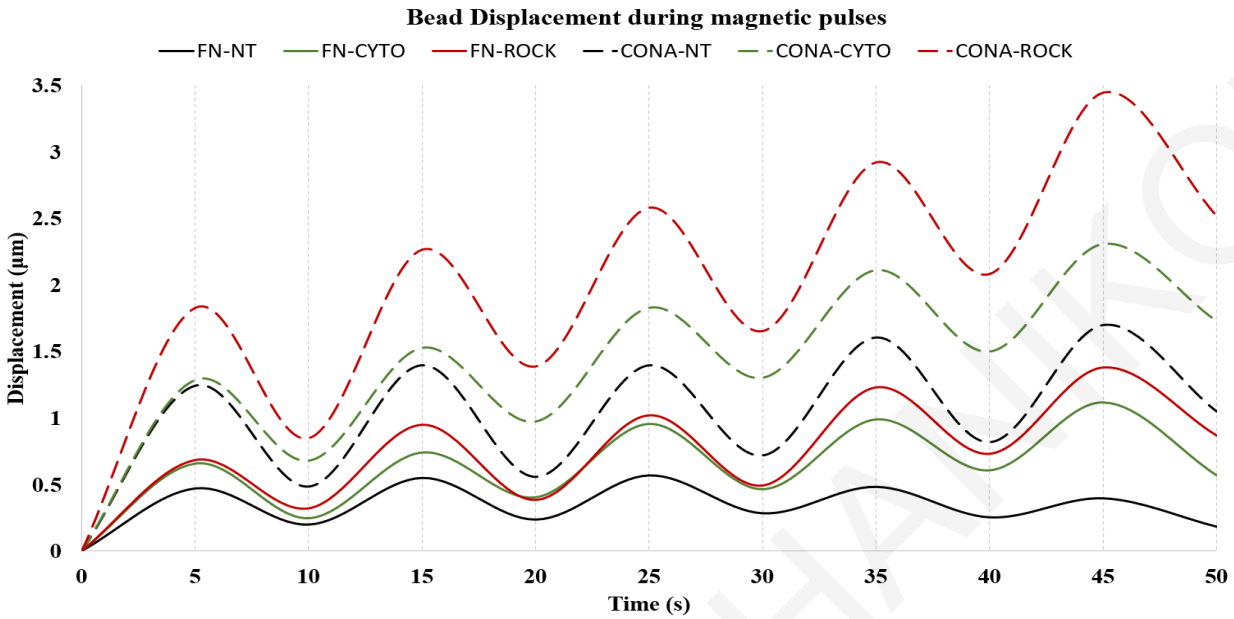

Figure 38: Schematic profiles of beads in each different scenario, constructed based on the mean values of normalize displacements and recoil.

These effects create an additive effect to the displacements, regardless of the magnitude of the normalize displacement, that as shown in many cases of these experiments **Figure 32**, the mean values, remain approximately the same except the FN-NT beads that show a gradient decrease. In **Figure 39** is the profile of the fibronectin coated beads that are attached on integrin receptors (FN-NT).

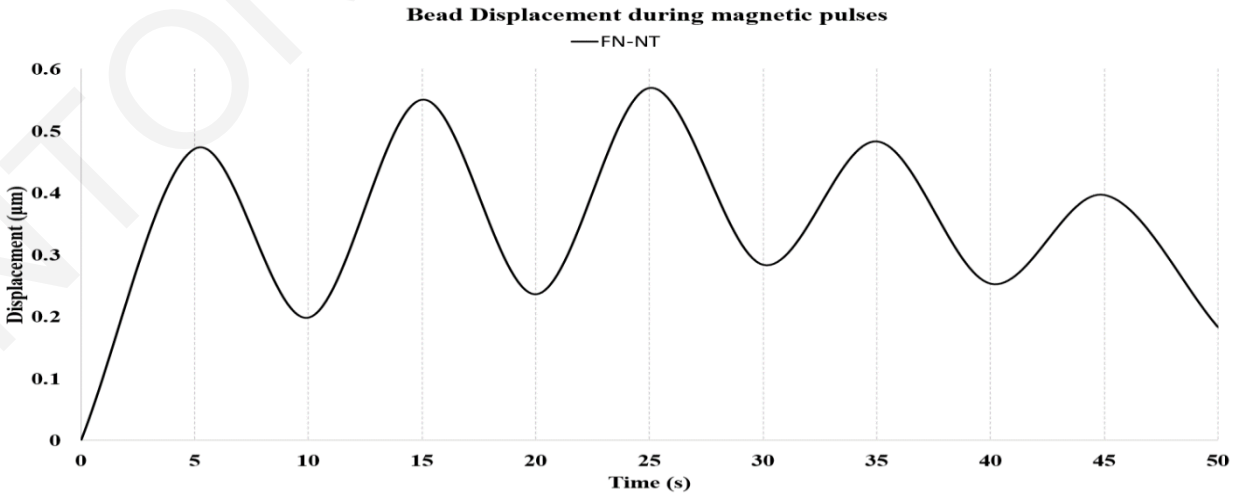

ANTONIS MICHAILOU

Figure 39: Profile for FN-NT beads that are attached on HeLa cells.

The FN-NT beads are experiencing a big displacement in the initial pulse. After 5 seconds, we have the removal of the magnetic field for 5 seconds, an incomplete return to the original position, and again upon activating the electromagnet the bead experiences another displacement and so on, leading to decreasing displacements and return of the bead to the relaxation position (10s).

At **Figure 40** is the pair comparison of the profiles of CONA-NT and FN-NT.

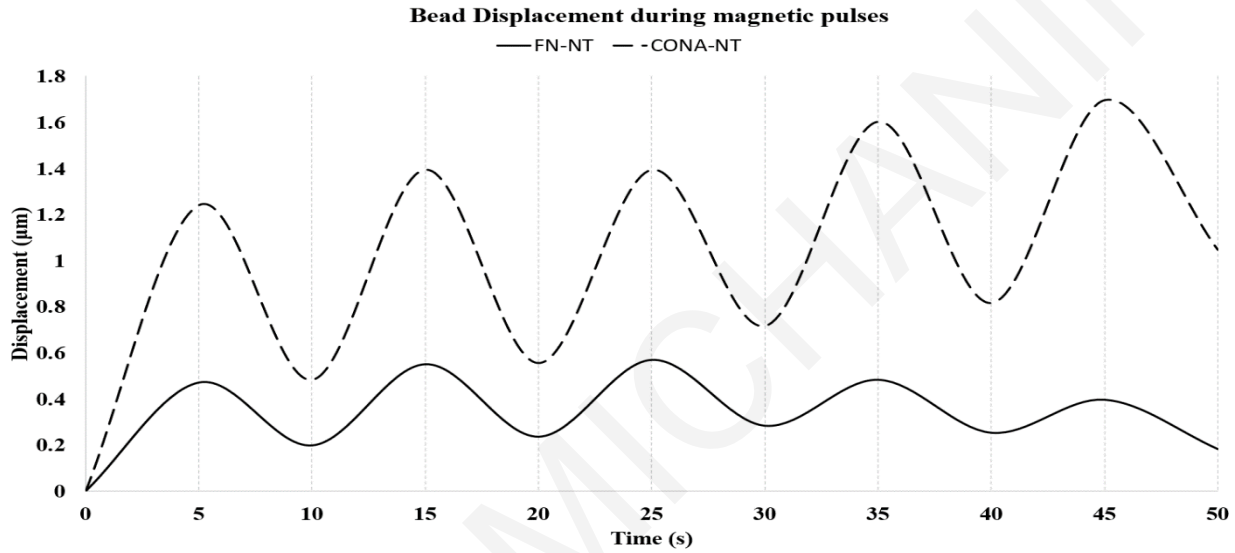

Figure 40: Bead profiles comparison for FN-NT and CONA-NT conjugated beads that are attached on HeLa cells.

The differences in the two profiles are showcasing what we previously stated that the CONA-NT beads that are not displaying specific attachment to the plasma membrane are following the same pattern across all pulses. In **Figure 41** are the pair comparisons between the fibronectin beads with and without the inhibitors. While FN-NT beads are displaying a significant decrease, the FN-CYTO and FN-ROCK profiles don't follow the same pattern as FN-NT beads. The addition of inhibitors drastically affects their overall movement through the pulses, as they exhibit larger displacements, showing the dependence of FN bead responses on the actin and actomyosin network.

ANTONIS MICHANIKOU

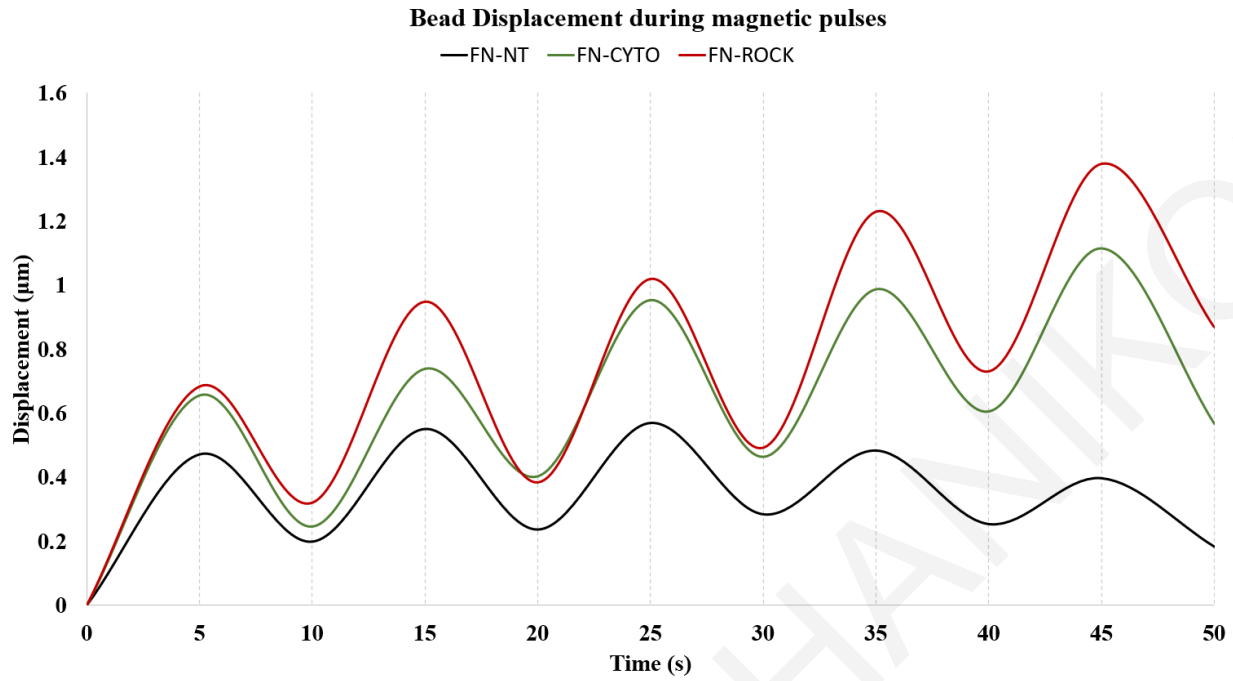

Figure 41: Bead profiles comparison for FN-NT, FN-CYTO and FN-ROCK conjugated beads that are attached on HeLa cells.

In **Figure 42** are the pair comparison of the CONA beads.

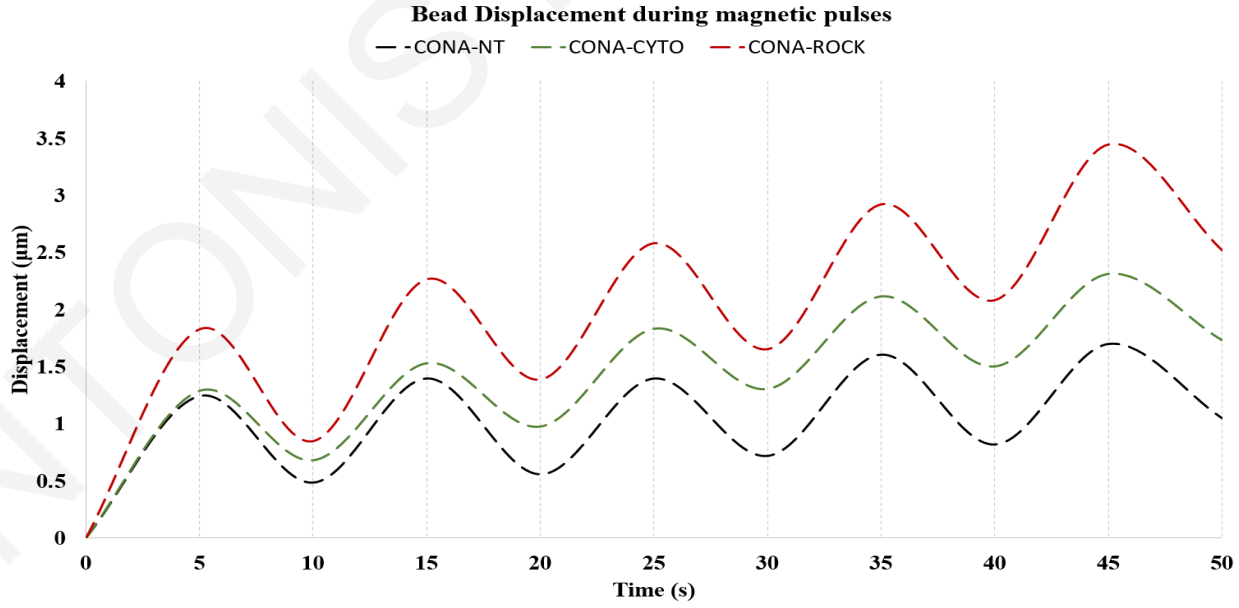

Figure 42: Bead profiles comparison for CONA-NT, CONA-CYTO and CONA-ROCK conjugated beads that are attached on HeLa cells.

ANTONIS MICHANIKOU

CONA beads are exhibiting similar profiles. As shown before the CONA-CYTO did not show increase displacements compared to CONA-NT, one would expect to follow similar profile as the CONA-NT, but it does not, the differences are not in the displacements but on the recoil displacement, the CONA-CYTO beads are experiencing less recoil upon displacement. An effect that may be due to experimental error.

The CONA-ROCK and CONA-NT are following the same profile, with only change in the amplitude of the displacement an effect that is attributed to the overall cell stiffness decrease that the rock inhibitor induces.

ANTONIS MICHANIKOU

DISCUSSION

Mechanical forces are continuously applied on cells, either intracellularly or extracellularly, mechanosensing is crucial for cell proliferation and differentiation. Cells can translate extracellular mechanical cues to intracellular biochemical signals. Mechanoreceptors like integrins can transduce ECM mechanical signals through the actin cytoskeleton and lead to the formation of focal adhesions and induce stiffening of the cell (Wang, Butler et al. 1993)

The main aim of this thesis was to study the local changes in the mechanical properties of the cell, elicited by mechanical stimulation of the plasma membrane through integrin dependent and independent mechanisms.

We constructed a nondirectional magnetic tweezer that was able to apply sufficient forces to the area of interest at a working distance allowing the avoidance of direct cell contact. Calibration of the magnetic tweezer on 4.5 μm superparamagnetic beads revealed that the custom tweezer set up was able to generate 13.6 nN of force at a distance from the electromagnet of 20 μm, result that agrees with previous similar designs (Kollmannsberger, Fabry 2007).

Experiments on polyacrylamide gels showcase the ability of the electromagnet to displace superparamagnetic beads (SpBs) on gels with different stiffness, resulting in decreasing displacements for stiffer substrates and showcase their elastic properties (Tse, Engler 2010).

Through initial experiments that we have tried to complete it was obvious that a great limitation of these devices was the lack of flexibility of a non-directional magnetic tweezer and also the live imaging process became extremely difficult as we had limitations with the structure and size of the magnetic tweezer which required very careful placement and limited its use in combination with an incubation system. These limitations could be overcome at least in part using beads with improved magnetic properties that would allow greater working distance or with the use of a more powerful electromagnet with better cooling. Nevertheless, the system we have established is an extremely valuable tool which allows unique experimentation that is not otherwise possible such as spatially restricted and specific mechanical stimulation using defined receptors on the cell surface.

Taking advantage of this custom build system we were able to address the main aim of our study by measuring displacements of (SpBs) in HeLa cells with and without treatment with inhibitors. Beads with fibronectin exhibit smaller displacements in higher force regimes compared to the

ANTONIS MICHANIKOU

ConA beads that are not only experiencing large displacements but can also be displaced using lower force. A result that showcases the direct link of the FN beads to the actin cytoskeleton. Fibronectin (FN) a known glycoprotein it's known to bound to integrins through its Arg-Gly-Asp (RGD) motif, although other possible sequences within fibronectin are reported to also to form connections (Pankov, Yamada 2002). Concanavalin A(ConA) a seed lectin, on the other hand has a low affinity and high specific binding on oligomers, monomers of mannose and glucose. The Fn beads revealed the stiffer nature of the actin cytoskeleton compared to the PM. Displacing FN beads requires greater force and displacements are significantly smaller than CONA beads under the same load. The link to the actin cytoskeleton using FN beads is also demonstrated by the greater contractility of such deformations with beads on some occasions moving beyond the initial point during recoil, an effect that was not observed when cells were treated with Rho inhibitor. This clearly shows that when the contractile force generating ability of the actomyosin network is lost, the mechanical recoil of the cell is impacted directly. Thus, it confirms not only that FN beads are directly linked to the actin cytoskeleton but also shows that the displacement and recoil of these beads are directly affected by the actomyosin network and its mechanical state. Importantly the same effect, was not seen when using CONA beads with or without inhibition. Interestingly beads that were conjugated with FN displayed a gradual decrease in their displacements resulting in an overall decrease of 61% from the initial displacement and when treated with the inhibitors the effect was not lost. This shows clearly that mechanical stimulation of integrin bound beads leads to stiffening of the cell through actin polymerization. The fact that this stiffening response is ablated upon cytochalasin treatment confirms that the cell responses are indeed actin based. The contractility inhibition shows that myosin is also necessary for these actin based responses. On the other hand, the ConA beads exhibited a decrease of -29% but was concentrated in the first pulses and was not gradual. These results show that mechanical stimulation of the PM also elicits cell stiffening responses that are integrin receptor independent. ConA beads displacement magnitude is only dependent on cortical stiffness and maybe affected by intermediate filaments through signaling from mechanosening channels on the plasma membrane. Our data also show that integrin independent responses to PM stimulation are faster and become saturated quickly since additional pulses do not result in further stiffening unlike integrin-based responses. It also suggests that responses when using FN beads must be the combined outcome of integrin dependent and independent mechanosensing.

ANTONIS MICHANKOU

However, the small displacements of FN beads compared to CONA makes it difficult to determine what the input of integrin independent based mechanosensing is in the case of the FN beads. Treatment with the inhibitors didn't show an effect on CONA beads as the same profiles were observed for the two inhibitors. This surprising result suggests that PM mechanical stimulation elicits actin independent stiffening which could be a result of changes in local lipid composition or subcortical polymerization of intermediate filaments. It could also potentially be elicited through increased local PM anchoring on the cytoskeleton however at this time we have no way to discriminate between these possible mechanisms. These results in combination with the loss of responses on FN beads also suggest that since FN bead responses are abolished with the use of cytochalasin the limited displacement of FN beads likely results in very limited integrin independent mechanosensing taking place. Furthermore, we were able to observe other characteristics of cells like plasticity that was previously reported by other laboratories working with magnetic tweezers (Bonakdar, Gerum et al. 2016).Thus PM deformation is not elastic, plastic effects are more profound in the ConA beads as they fail to return to their initial position during the relaxation phase of the first pulse, an effect that is maintained when treating with the inhibitors. On the contrary Fn bead displacements are plastic initially, however they manage to return to first recoil position by the end of the 5th Pulse, as actin and myosin responses are in place, an effect that is not observed when treating with the inhibitors, thus affecting actin polymerization and actomyosin contractility.

Cells in the human body are constantly experiencing changes in applied forces, mechanosensing and translation of these cues to biochemical signals, help cells change shape, adapt and proliferate. Integrin activation upon mechanical stress and stiffening of the plasma membrane through the actin cytoskeleton was also observed in previous experiments (Bausch, Hellerer et al. 2001, Wang, Butler et al. 1993). While the results provided are in accordance with other studies, they are subject to several limitations. First, the experiments led to a small sample size that affect the analysis and in some cases was difficult to conclude, also the unidirectional design of the magnetic tweezer was a limiting factor on live imaging process for these experiments. While other similar designs that are multidirectional, they solve the flexibility issue but are bulky devices that affect the imaging process from another angle. Optical tweezers on the other hand are flexible and the more precise of all the designs, but are not an easily affordable equipment,

ANTONIS MICHANKOU

phototoxicity is a constant problem with these devices, and the magnitude of force they can induce is magnitudes lower than the magnetic tweezers (Kollmannsberger, Fabry 2007, Kah, Dürrbeck et al. 2020). The limitation of the unidirectional design of the magnetic tweezer can be addressed by using self-rotating stages, additionally designing a custom-made attachment mechanism for the magnetic tweezer to the micromanipulator, can stabilize and offer more precise movements for the experiments.

To conclude, we have established a custom magnetic tweezer with the ability to exert sufficient forces to deform the plasma membrane, we have applied this system and shown that upon applied force to the plasma membrane through integrin dependent and independent mechanisms it let to the stiffening of the PM. Experience drawn from working with the established system can facilitate future experiments to address other force dependent biological process like bending of the primary cilium or to promote tension driven integrin activation at ectopic adherens junctions.

ANTONIS MICHANIKOU

ABBREVIATIONS

ABBREVIATION	MEANING
AWG	American wire gauge
Pa	Pascal
CONA	Concanavalin A
FN	Fibronectin
FN-NT	Fibronectin Beads- No Treatment
FN-CYTO	Fibronectin Beads- Cytochalasin D
FN- ROCK	Fibronectin Beads- RhO kinase inhibitor
CONA-NT	Concanavalin A Beads- No Treatment
CONA-CYTO	Concanavalin A Beads- Cytochalasin D
CONA-ROCK	Concanavalin A Beads- RhO kinase inhibitor
TM	Transmembrane domain
ATP	Adenosine 5′-triphosphate
ADP	Adenosine diphosphate
ADF	Actin-depolymerization factor
NM II	Non- Muscle Myosin II
ELCs	Essential light chains
RLCs	Regulatory light chains
IF	Intermediate filaments

ANTONIS MICHANIKOU

BIBLIOGRAPHY

AGUILAR-CUENCA, R., LLORENTE-GONZÁLEZ, C., CHAPMAN, J.R., TALAYERO, V.C., GARRIDO-CASADO, M., DELGADO-ARÉVALO, C., MILLÁN-SALANOVA, M., SHABANOWITZ, J., HUNT, D.F. and SELLERS, J.R., 2020. Tyrosine phosphorylation of the myosin regulatory light chain controls non-muscle myosin II assembly and function in migrating cells. *Current Biology*, **30**(13), pp. 2446-2458. e6.

ANTHIS, N.J. and CAMPBELL, I.D., 2011. The tail of integrin activation. *Trends in biochemical sciences*, **36**(4), pp. 191-198.

ARPAIA, P., BURROWS, P.N., BUZIO, M., GOHIL, C., PENTELLA, M. and SCHULTE, D., 2021. Magnetic characterization of Mumetal® for passive shielding of stray fields down to the nano-Tesla level. *Nuclear Instruments and Methods in Physics Research Section A: Accelerators, Spectrometers, Detectors and Associated Equipment*, **988**, pp. 164904.

BACHMANN, M., KUKKURAINEN, S., HYTÖNEN, V.P. and WEHRLE-HALLER, B., 2019. Cell adhesion by integrins. *Physiological Reviews*, **99**(4), pp. 1655-1699.

BARCZYK, M., CARRACEDO, S. and GULLBERG, D., 2010. Integrins. *Cell and tissue research*, **339**(1), pp. 269-280.

BAUSCH, A.R., HELLERER, U., ESSLER, M., AEPFELBACHER, M. and SACKMANN, E., 2001. Rapid stiffening of integrin receptor-actin linkages in endothelial cells stimulated with thrombin: a magnetic bead microrheology study. *Biophysical journal*, **80**(6), pp. 2649-2657.

BERGERT, M., CHANDRADOSS, S.D., DESAI, R.A. and PALUCH, E., 2012. Cell mechanics control rapid transitions between blebs and lamellipodia during migration. *Proceedings of the National Academy of Sciences*, **109**(36), pp. 14434-14439.

BERNABÉ-RUBIO, M., ANDRÉS, G., CASARES-ARIAS, J., FERNÁNDEZ-BARRERA, J., RANGEL, L., REGLERO-REAL, N., GERSHLICK, D.C., FERNÁNDEZ, J.J., MILLÁN, J. and CORREAS, I., 2016. Novel role for the midbody in primary ciliogenesis by polarized epithelial cells. *Journal of Cell Biology*, **214**(3), pp. 259-273.

BLANCHOIN, L., BOUJEMAA-PATERSKI, R., SYKES, C. and PLASTINO, J., 2014. Actin dynamics, architecture, and mechanics in cell motility. *Physiological Reviews*, **94**(1), pp. 235-263.

BONAKDAR, N., GERUM, R., KUHN, M., SPÖRRER, M., LIPPERT, A., SCHNEIDER, W., AIFANTIS, K.E. and FABRY, B., 2016. Mechanical plasticity of cells. *Nature materials*, **15**(10), pp. 1090-1094.

ANTONIS MICHANIKOU

BUCK, C.A. and HORWITZ, A., 1987. Integrin, a transmembrane glycoprotein complex mediating cell–substratum adhesion. *Journal of cell science,* **1987**(Supplement_8), pp. 231-250.

BUGYI, B. and CARLIER, M., 2010. Control of actin filament treadmilling in cell motility. *Annual review of biophysics,* **39**(1), pp. 449-470.

BURRIDGE, K. and GUILLUY, C., 2016. Focal adhesions, stress fibers and mechanical tension. *Experimental cell research,* **343**(1), pp. 14-20.

CALDWELL, J.E., HEISS, S.G., MERMALL, V. and COOPER, J.A., 1989. Effects of CapZ, an actin-capping protein of muscle, on the polymerization of actin. *Biochemistry,* **28**(21), pp. 8506-8514.

CAO, L., NICOSIA, J., LAROUCHE, J., ZHANG, Y., BACHMAN, H., BROWN, A.C., HOLMGREN, L. and BARKER, T.H., 2017. Detection of an integrin-binding mechanoswitch within fibronectin during tissue formation and fibrosis. *ACS nano,* **11**(7), pp. 7110-7117.

CARLIER, M. and PANTALONI, D., 1988. Binding of phosphate to F-ADP-actin and role of F-ADP-Pi-actin in ATP-actin polymerization. *Journal of Biological Chemistry,* **263**(2), pp. 817-825.

CHEN, Y., JU, L., RUSHDI, M., GE, C. and ZHU, C., 2017. Receptor-mediated cell mechanosensing. *Molecular biology of the cell,* **28**(23), pp. 3134-3155.

CHOUHAN, B., DENESYUK, A., HEINO, J., JOHNSON, M.S. and DENESSIOUK, K., 2011. Conservation of the human integrin-type beta-propeller domain in bacteria. *PloS one,* **6**(10), pp. e25069.

CLAUSEN, M.V., JARERATTANACHAT, V., CARPENTER, E.P., SANSOM, M.S. and TUCKER, S.J., 2017. Asymmetric mechanosensitivity in a eukaryotic ion channel. *Proceedings of the National Academy of Sciences,* **114**(40), pp. E8343-E8351.

COOPER, G.M., 2000. Structure and organization of actin filaments. *The cell: a molecular approach,* **2**.

CRAIG, D., GAO, M., SCHULTEN, K. and VOGEL, V., 2004. Structural insights into how the MIDAS ion stabilizes integrin binding to an RGD peptide under force. *Structure,* **12**(11), pp. 2049-2058.

DANEN, E.H., 2013. Integrins: An overview of structural and functional aspects. *Madame Curie Bioscience Database [Internet],* .

DE BELLY, H., PALUCH, E.K. and CHALUT, K.J., 2022. Interplay between mechanics and signalling in regulating cell fate. *Nature Reviews Molecular Cell Biology,* , pp. 1-16.

ANTONIS MICHAILIKOU

DOMINGUEZ, R. and HOLMES, K.C., 2011. Actin structure and function. *Annual review of biophysics*, **40**, pp. 169-186.

DURER, Z.A.O., KUDRYASHOV, D.S., SAWAYA, M.R., ALTENBACH, C., HUBBELL, W. and REISLER, E., 2012. Structural states and dynamics of the D-loop in actin. *Biophysical journal*, **103**(5), pp. 930-939.

DUTOUR-PROVENZANO, G. and ETIENNE-MANNEVILLE, S., 2021. Intermediate filaments. *Current Biology*, **31**(10), pp. R522-R529.

EDWARDS, M., ZWOLAK, A., SCHAFER, D.A., SEPT, D., DOMINGUEZ, R. and COOPER, J.A., 2014. Capping protein regulators fine-tune actin assembly dynamics. *Nature reviews Molecular cell biology*, **15**(10), pp. 677-689.

ERUSAPPAN, P., ALAM, J., LU, N., ZELTZ, C. and GULLBERG, D., 2019. Integrin α11 cytoplasmic tail is required for FAK activation to initiate 3D cell invasion and ERK-mediated cell proliferation. *Scientific reports*, **9**(1), pp. 1-12.

FISCHER, S., WINDSHUGEL, B., HORAK, D., HOLMES, K.C. and SMITH, J.C., 2005. Structural mechanism of the recovery stroke in the myosin molecular motor. *Proceedings of the National Academy of Sciences of the United States of America*, **102**(19), pp. 6873-6878.

GAHMBERG, C.G., GRÖNHOLM, M. and MADHAVAN, S., 2022. Regulation of Dynamic Cell Adhesion by Integrin-Integrin Crosstalk. *Cells*, **11**(10), pp. 1685.

GEISLER, F. and LEUBE, R.E., 2016. Epithelial intermediate filaments: guardians against microbial infection? *Cells*, **5**(3), pp. 29.

GOLDMAN, R.D., GRIN, B., MENDEZ, M.G. and KUCZMARSKI, E.R., 2008. Intermediate filaments: versatile building blocks of cell structure. *Current opinion in cell biology*, **20**(1), pp. 28-34.

HADJISAVVA, R., ANASTASIOU, O., IOANNOU, P.S., ZHELTKOVA, M. and SKOURIDES, P.A., 2022. Adherens junctions stimulate and spatially guide integrin activation and extracellular matrix deposition. *Cell Reports*, **40**(3), pp. 111091.

HAN, Y. and ALVAREZ-BUYLLA, A., 2010. Role of primary cilia in brain development and cancer. *Current opinion in neurobiology*, **20**(1), pp. 58-67.

HERRMANN, H., STRELKOV, S.V., BURKHARD, P. and AEBI, U., 2009. Intermediate filaments: primary determinants of cell architecture and plasticity. *The Journal of clinical investigation*, **119**(7), pp. 1772-1783.

HIGGS, H., 2001. Getting down to basics with actin. *Nature cell biology*, **3**(8), pp. E189.

ANTONIS MICHANKOU

HIRATA, H., GUPTA, M., VEDULA, S.R.K., LIM, C.T., LADOUX, B. and SOKABE, M., 2015. Actomyosin bundles serve as a tension sensor and a platform for ERK activation. *EMBO reports,* **16**(2), pp. 250-257.

HOHMANN, T. and DEHGHANI, F., 2019. The cytoskeleton—a complex interacting meshwork. *Cells,* **8**(4), pp. 362.

HYNES, R.O., 2002. Integrins: bidirectional, allosteric signaling machines. *Cell,* **110**(6), pp. 673-687.

JACOB, J.T., COULOMBE, P.A., KWAN, R. and OMARY, M.B., 2018. Types I and II Keratin Intermediate Filaments. *Cold Spring Harbor perspectives in biology,* **10**(4), pp. a018275. doi: 10.1101/cshperspect.a018275.

KAH, D., DÜRRBECK, C., SCHNEIDER, W., FABRY, B. and GERUM, R.C., 2020. High-force magnetic tweezers with hysteresis-free force feedback. *Biophysical journal,* **119**(1), pp. 15-23.

KOLLMANNSBERGER, P. and FABRY, B., 2007. BaHigh-force magnetic tweezers with force feedback for biological applications. *Review of Scientific Instruments,* **78**(11), pp. 114301.

KUDRYASHOV, D.S. and REISLER, E., 2013. ATP and ADP actin states. *Biopolymers,* **99**(4), pp. 245-256.

LEHTIMÄKI, J.I., RAJAKYLÄ, E.K., TOJKANDER, S. and LAPPALAINEN, P., 2021. Generation of stress fibers through myosin-driven reorganization of the actin cortex. *Elife,* **10**, pp. e60710.

LIETHA, D. and IZARD, T., 2020. Roles of membrane domains in integrin-mediated cell adhesion. *International Journal of Molecular Sciences,* **21**(15), pp. 5531.

MEHRBOD, M., TRISNO, S. and MOFRAD, M.R., 2013. On the activation of integrin αIIbβ3: outside-in and inside-out pathways. *Biophysical journal,* **105**(6), pp. 1304-1315.

MORSE, E.M., BRAHME, N.N. and CALDERWOOD, D.A., 2014. Integrin cytoplasmic tail interactions. *Biochemistry,* **53**(5), pp. 810-820.

MOULD, A.P., BARTON, S.J., ASKARI, J.A., CRAIG, S.E. and HUMPHRIES, M.J., 2003. Role of ADMIDAS cation-binding site in ligand recognition by integrin alpha 5 beta 1. *The Journal of biological chemistry,* **278**(51), pp. 51622-51629.

OJIMA, K., 2019. Myosin: Formation and maintenance of thick filaments. *Animal Science Journal,* **90**(7), pp. 801-807.

ANTONIS MICHANIKOU

OXVIG, C. and SPRINGER, T.A., 1998. Experimental support for a beta-propeller domain in integrin alpha-subunits and a calcium binding site on its lower surface. *Proceedings of the National Academy of Sciences of the United States of America,* **95**(9), pp. 4870-4875.

PANKOV, R. and YAMADA, K.M., 2002. Fibronectin at a glance. *Journal of cell science,* **115**(20), pp. 3861-3863.

PANNEKOEK, W., DE ROOIJ, J. and GLOERICH, M., 2019. Force transduction by cadherin adhesions in morphogenesis. *F1000Research,* **8**, pp. 10.12688/f1000research.18779.1. eCollection 2019.

PARISI, L., TOFFOLI, A., GHEZZI, B., MOZZONI, B., LUMETTI, S. and MACALUSO, G.M., 2020. A glance on the role of fibronectin in controlling cell response at biomaterial interface. *Japanese dental science review,* **56**(1), pp. 50-55.

PASZEK, M.J., ZAHIR, N., JOHNSON, K.R., LAKINS, J.N., ROZENBERG, G.I., GEFEN, A., REINHART-KING, C.A., MARGULIES, S.S., DEMBO, M. and BOETTIGER, D., 2005. Tensional homeostasis and the malignant phenotype. *Cancer cell,* **8**(3), pp. 241-254.

POLACHECK, W.J. and CHEN, C.S., 2016. Measuring cell-generated forces: a guide to the available tools. *Nature methods,* **13**(5), pp. 415-423.

POLLARD, T.D., 1984. Polymerization of ADP-actin. *The Journal of cell biology,* **99**(3), pp. 769-777.

POLLARD, T.D., BLANCHOIN, L. and MULLINS, R.D., 2000. Molecular mechanisms controlling actin filament dynamics in nonmuscle cells. *Annual Review of Biophysics and Biomolecular Structure,* **29**, pp. 545-576.

RAHMANI, H., MA, W., HU, Z., DANESHPARVAR, N., TAYLOR, D.W., MCCAMMON, J.A., IRVING, T.C., EDWARDS, R.J. and TAYLOR, K.A., 2021. The myosin II coiled-coil domain atomic structure in its native environment. *Proceedings of the National Academy of Sciences,* **118**(14), pp. e2024151118.

RIDONE, P., VASSALLI, M. and MARTINAC, B., 2019. Piezo1 mechanosensitive channels: what are they and why are they important. *Biophysical reviews,* **11**(5), pp. 795-805.

ROCA-CUSACHS, P., CONTE, V. and TREPAT, X., 2017. Quantifying forces in cell biology. *Nature cell biology,* **19**(7), pp. 742-751.

RUIZ-GÓMEZ, A., MOLNAR, C., HOLGUÍN, H., MAYOR JR, F. and DE CELIS, J.F., 2007. The cell biology of Smo signalling and its relationships with GPCRs. *Biochimica et Biophysica Acta (BBA)-Biomembranes,* **1768**(4), pp. 901-912.

SAMUEL, M.S., LOPEZ, J.I., MCGHEE, E.J., CROFT, D.R., STRACHAN, D., TIMPSON, P., MUNRO, J., SCHRÖDER, E., ZHOU, J. and BRUNTON, V.G., 2011. Actomyosin-mediated

ANTONIS MICHAILIKOU

cellular tension drives increased tissue stiffness and β-catenin activation to induce epidermal hyperplasia and tumor growth. *Cancer cell,* **19**(6), pp. 776-791.

SANTA-CRUZ MATEOS, C., VALENCIA-EXPÓSITO, A., PALACIOS, I.M. and MARTÍN-BERMUDO, M.D., 2020. Integrins regulate epithelial cell shape by controlling the architecture and mechanical properties of basal actomyosin networks. *PLoS genetics,* **16**(6), pp. e1008717.

SHATTIL, S.J., KIM, C. and GINSBERG, M.H., 2010. The final steps of integrin activation: the end game. *Nature reviews Molecular cell biology,* **11**(4), pp. 288-300.

SHEKHAR, S. and CARLIER, M., 2017. Enhanced depolymerization of actin filaments by ADF/cofilin and monomer funneling by capping protein cooperate to accelerate barbed-end growth. *Current Biology,* **27**(13), pp. 1990-1998. e5.

SHOJI, K., OHASHI, K., SAMPEI, K., OIKAWA, M. and MIZUNO, K., 2012. Cytochalasin D acts as an inhibitor of the actin–cofilin interaction. *Biochemical and biophysical research communications,* **424**(1), pp. 52-57.

SHUTOVA, M., YANG, C., VASILIEV, J.M. and SVITKINA, T., 2012. Functions of nonmuscle myosin II in assembly of the cellular contractile system. *PloS one,* **7**(7), pp. e40814.

SKAU, C.T. and WATERMAN, C.M., 2015. Specification of Architecture and Function of Actin Structures by Actin Nucleation Factors. *Annual review of biophysics,* **44**, pp. 285-310.

SUN, H.Q., WOOTEN, D.C., JANMEY, P.A. and YIN, H.L., 1994. The actin side-binding domain of gelsolin also caps actin filaments. Implications for actin filament severing. *The Journal of biological chemistry,* **269**(13), pp. 9473-9479.

SUN, S., FISHER, R.L., BOWSER, S.S., PENTECOST, B.T. and SUI, H., 2019. Three-dimensional architecture of epithelial primary cilia. *Proceedings of the National Academy of Sciences,* **116**(19), pp. 9370-9379.

SYAMALADEVI, D.P., SPUDICH, J.A. and SOWDHAMINI, R., 2012. Structural and functional insights on the Myosin superfamily. *Bioinformatics and biology insights,* **6**, pp. BBI. S8451.

TAKADA, Y., YE, X. and SIMON, S., 2007. The integrins. *Genome biology,* **8**(5), pp. 1-9.

TAKAGI, J., PETRE, B.M., WALZ, T. and SPRINGER, T.A., 2002. Global conformational rearrangements in integrin extracellular domains in outside-in and inside-out signaling. *Cell,* **110**(5), pp. 599-611.

TANASE, M., BIAIS, N. and SHEETZ, M., 2007. Magnetic tweezers in cell biology. *Methods in cell biology,* **83**, pp. 473-493.

ANTONIS MICHANIKOU

TOYOSHIMA, Y.Y., KRON, S.J., MCNALLY, E.M., NIEBLING, K.R., TOYOSHIMA, C. and SPUDICH, J.A., 1987. Myosin subfragment-1 is sufficient to move actin filaments in vitro. *Nature,* **328**(6130), pp. 536-539.

TRIVEDI, D.V., NAG, S., SPUDICH, A., RUPPEL, K.M. and SPUDICH, J.A., 2020. The Myosin Family of Mechanoenzymes: From Mechanisms to Therapeutic Approaches. *Annual Review of Biochemistry,* **89**, pp. 667-693.

TSE, J.R. and ENGLER, A.J., 2010. Preparation of hydrogel substrates with tunable mechanical properties. *Current protocols in cell biology,* **47**(1), pp. 10.16. 1-10.16. 16.

VICENTE-MANZANARES, M., MA, X., ADELSTEIN, R.S. and HORWITZ, A.R., 2009. Non-muscle myosin II takes centre stage in cell adhesion and migration. *Nature reviews Molecular cell biology,* **10**(11), pp. 778-790.

VILFAN, I.D., LIPFERT, J., KOSTER, D., LEMAY, S. and DEKKER, N., 2009. Magnetic tweezers for single-molecule experiments. *Handbook of single-molecule biophysics, ,* pp. 371-395.

VISA, N. and PERCIPALLE, P., 2010. Nuclear functions of actin. *Cold Spring Harbor perspectives in biology,* **2**(4), pp. a000620.

WAKATSUKI, T., SCHWAB, B., THOMPSON, N.C. and ELSON, E.L., 2001. Effects of cytochalasin D and latrunculin B on mechanical properties of cells. *Journal of cell science,* **114**(5), pp. 1025-1036.

WANG, N., BUTLER, J.P. and INGBER, D.E., 1993. Mechanotransduction across the cell surface and through the cytoskeleton. *Science (New York, N.Y.),* **260**(5111), pp. 1124-1127.

WATANABE, N., MADAULE, P., REID, T., ISHIZAKI, T., WATANABE, G., KAKIZUKA, A., SAITO, Y., NAKAO, K., JOCKUSCH, B.M. and NARUMIYA, S., 1997. p140mDia, a mammalian homolog of Drosophila diaphanous, is a target protein for Rho small GTPase and is a ligand for profilin. *The EMBO journal,* **16**(11), pp. 3044-3056.

WEGENER, K.L. and CAMPBELL, I.D., 2008. Transmembrane and cytoplasmic domains in integrin activation and protein-protein interactions. *Molecular membrane biology,* **25**(5), pp. 376-387.

XIONG, J., STEHLE, T., DIEFENBACH, B., ZHANG, R., DUNKER, R., SCOTT, D.L., JOACHIMIAK, A., GOODMAN, S.L. and ARNAOUT, M.A., 2001. Crystal structure of the extracellular segment of integrin αVβ3. *Science,* **294**(5541), pp. 339-345.

XIONG, J., STEHLE, T., ZHANG, R., JOACHIMIAK, A., FRECH, M., GOODMAN, S.L. and ARNAOUT, M.A., 2002. Crystal structure of the extracellular segment of integrin αVβ3 in complex with an Arg-Gly-Asp ligand. *Science,* **296**(5565), pp. 151-155.

ANTONIS MICHANIKOU

XUE, F., COX, C.D., BAVI, N., ROHDE, P.R., NAKAYAMA, Y. and MARTINAC, B., 2020. Membrane stiffness is one of the key determinants of E. coli MscS channel mechanosensitivity. *Biochimica et Biophysica Acta (BBA)-Biomembranes*, **1862**(5), pp. 183203.

YAP, A.S., DUSZYC, K. and VIASNOFF, V., 2018. Mechanosensing and Mechanotransduction at Cell-Cell Junctions. *Cold Spring Harbor perspectives in biology*, **10**(8), pp. a028761. doi: 10.1101/cshperspect.a028761.

YOUSEFI, H., VATANMAKANIAN, M., MAHDIANNASSER, M., MASHOURI, L., ALAHARI, N.V., MONJEZI, M.R., ILBEIGI, S. and ALAHARI, S.K., 2021. Understanding the role of integrins in breast cancer invasion, metastasis, angiogenesis, and drug resistance. *Oncogene*, **40**(6), pp. 1043-1063.

ZWEIFEL, M.E. and COURTEMANCHE, N., 2020. Profilin's affinity for formin regulates the availability of filament ends for actin monomer binding. *Journal of Molecular Biology*, **432**(24), pp. 166688.

ANTONIS MICHAILIKOU